HHS Public Access

Author manuscript

Nat Cell Biol. Author manuscript; available in PMC 2020 July 06.

Published in final edited form as:

Nat Cell Biol. 2020 January ; 22(1): 97–107. doi:10.1038/s41556-019-0443-x.

P120-catenin dependent collective brain infiltration by glioma cell networks

Pavlo G. Gritsenko[1], **Nader Atlasy**[2,3], **Cindy E.J. Dieteren**[1,4], **Anna C. Navis**[5], **Jan-Hendrik Venhuizen**[1], **Cornelia Veelken**[1], **Dirk Schubert**[6], **Amparo Acker-Palmer**[7,8], **Bart A. Westerman**[9], **Thomas Wurdinger**[9], **William Leenders**[10], **Pieter Wesseling**[11,12], **Hendrik G. Stunnenberg**[2,12], **Peter Friedl**[1,13,14]

[1]Department of Cell Biology, Radboud University Medical Center, Nijmegen, The Netherlands [2]Department of Molecular Biology, Radboud University, Nijmegen, The Netherlands [3]Center for Molecular Medicine, University Medical Center, Utrecht, The Netherlands [4]Protinhi Therapeutics, Nijmegen, the Netherlands [5]Department of Medical Biochemistry and Biophysics, Karolinska Institutet, Stockholm, Sweden [6]Cognitive Neuroscience Department, Donders Institute, Radboud University Medical Center, Nijmegen, The Netherlands [7]Institute of Cell Biology and Neuroscience and BMLS, Goethe University Frankfurt, Germany [8]Max Planck Institute for Brain Research, Max von Laue Strasse 4, 60438 Frankfurt, Germany [9]Department of Neurosurgery, VU University Medical Center, Amsterdam, The Netherlands [10]Department of Biochemistry, Radboud University Medical Center, Nijmegen, The Netherlands [11]Department of Pathology, Amsterdam University Medical Centers/VUmc and Brain Tumor Center Amsterdam, Amsterdam, The Netherlands [12]Princess Máxima Center for Pediatric Oncology, Utrecht, The Netherlands [13]The University of Texas MD Anderson Cancer Center, Houston, Texas, USA [14]Cancer Genomics Center (Cancergenomics.nl), Utrecht, The Netherlands

Abstract

Diffuse brain infiltration by glioma cells causes detrimental disease progression, however its multicellular coordination is poorly understood. We here show that glioma cells infiltrate brain collectively, as multicellular networks. Contacts between moving glioma cells were adaptive epithelial-like or filamentous junctions stabilized by N-cadherin, β-catenin and p120-catenin, which underwent kinetic turn-over, transmitted intercellular calcium transients and mediated directional persistence. Downregulation of p120-catenin compromised cell-cell interaction and communication, disrupted collective networks, and both the cadherin and RhoA binding domains of p120-catenin were required for network formation and migration. Deregulating p120-catenin further prevented diffuse glioma cell infiltration of the mouse brain with marginalized

Correspondence to: Peter.Friedl@radboudumc.nl pfriedl@mdanderson.org.

Author contributions

P.G.G., N.A., C.E.J.D., W.L., P.W., A.A.-P., B.A.W., T.W., H.G.S. and P.F. designed the experiments and interpreted the data. P.G.G., N.A., C.E.J.D., A.C.N., J.-H.V., C.V., B.A.W. and D.S. performed experiments and quantitatively analyzed the data. P.G.G. and P.F. wrote the paper. All authors read and corrected the manuscript.

Disclosure of potential conflicts of interests

No potential conflicts of interests were disclosed.

microlesions as outcome. Transcriptomics analysis identified p120-catenin as upstream regulator of neurogenesis and cell cycle pathways and predictor of poor clinical outcome in glioma patients. Collective glioma networks infiltrating the brain thus depend on adherens junctions dynamics the targeting of which may offer an unanticipated strategy to halt glioma progression.

INTRODUCTION

Diffuse gliomas are invasive and fatal primary brain tumors, with astrocytic and oligodendroglial molecular subtypes and glioblastoma as the most aggressive astrocytic variant[1]. Driver mutations of gliomas include isocitrate dehydrogenase (IDH), RTK/RAS/PI3K, p53 and RB pathways, and δ2-catenin, causing cell reprogramming by deranging cell cycle, metabolic programs, cell-cell interaction and migration[2–5]. Diffuse gliomas develop outstanding invasion and survival capability and continue to infiltrate brain even during high-dose chemo- and radiation therapy[6,7]. Glioma invasion, growth and resistance programs cooperate with epithelial-to-mesenchymal transition (EMT)-like plasticity programs[8,9]. However, how glioma invasion and survival programs cooperate, and whether they occur in a cell-autonomous manner or depend upon crosstalk between glioma cells themselves or non-neoplastic glial or neuronal cells remains unclear[10].

Glioma cells infiltrate brain tissue as individually moving cells by at least two topographic and likely interconvertible programs, including perivascular invasion, along the vascular basement membrane, and diffuse infiltration of the brain parenchyma, along extracellular matrix, nerve and astrocytic tracts[10,11]. Besides single-cell dissemination, multicellular networks with filamentous microtubes were recently identified to connect glioma cells in developing and established glioma lesions in the human brain and glioma mouse models[12]. Through gap junctions and propagating Ca^{2+} waves, glioma cells form a functional syncytium, similarly to astrocytic networks, and thereby maintain resistance to experimental radiation therapy[12]. Whether intercellular connections locally immobilize glioma cells or, instead, favor brain invasion remains unresolved.

To address whether glioma networks hinder or rather support glioma cell migration and brain infiltration, we here applied organotypic there-dimensional (3D) culture and in vivo analyses and identified collective network invasion deployed by glioma cells. We further identify p120-catenin dependent adherens junctions (AJs) as a central hub enabling dynamic cell-cell interactions and network infiltration into brain parenchyma.

RESULTS

Network organization of glioma lesions in vivo

To revisit the network concept in invasive glioma[12], we mapped the 3D microanatomy of the glioma invasion zone of clinical samples (Supplementary Table 1). Conventional single-slice pathology reveals spatially dispersed cell bodies with small filamentous protrusions and little sign of intercellular connectivity. 3D image reconstruction using immunofluorescent staining for $IDH1^{R132H}$ and nestin allowed to discriminate glioma from non-neoplastic glial and other brain cells[13], revealing extensive multicellular glioma cell networks in both tumor

center and diffusely infiltrating margins (Extended Data Fig. 1a–f and Supplementary Video 1). Glioma networks were present in low-grade astrocytomas and glioblastomas with wild-type and mutant IDH1 (R132H), indicating relevance across glioma subtypes. Two morphological variants of cell-cell junctions were identified, (i) filamentous networks between glioma cells reaching deeply into the brain parenchyma (Extended Data Fig. 1a, f) and (ii) compact linear junctions present in collective invasion strands extending along the perivascular niche (Extended Data Fig. 1g, h).

We then implanted patient-derived glioma xenograft-(PDX-) E-98 and E-468 cells[14] with respective proneural and mesenchymal genetic signatures[15] (Extended Data Fig. 2a) into the mouse brain. Both PDXs diffusely infiltrated both grey and white matter of the mouse brain as multicellular networks (Fig. 1a), consisting of dispersed cell bodies connected by an average of 4–8 branched dendritic filaments (Fig. 1c; Supplementary Videos 2, 3). Filaments retained anatomical contacts to an average of 4 to 6 (total range 1 to >10) neighboring glioma cells in 3D space over distances between 10 up to 200 μm (Fig. 1b, d). Dendritic protrusions between glioma cells contained microtubules and the intermediate filament proteins vimentin and nestin (Extended Data Fig. 1i; Supplementary Video 4), in morphological reminiscence of filamentous junctions between astrocytes or neuronal networks during morphogenesis[16,17]. Besides multicellular networks, perivascular invasion zones comprised either directly adjacent cells bordered by epithelial-like AJs (E-98), or sparsely distributed cells (E-468) connected with filamentous junctions (Fig. 1e–h). Thus, both PDX models developed interstitial and perivascular brain invasion and for both routes the majority of glioma cells retained cell-cell junctions, similar to multicellular networks in other glioma models[12].

Collective invasion of glioma cell networks

The abundance of morphologically diverse cell-cell junctions between glioma cells during brain infiltration is a morphological indication of collective invasion[18], which depends on adhesive cell-cell junctions and mechanochemical cooperativity between moving cells[18–20]. Using complementary 3D in vitro models mimicking brain invasion[21], we next tested whether cell-cell junctions hinder or support tissue infiltration by glioma cells. Glioma cells invaded as compact capillary-like strands along the interphase between two layers of reconstituted basement membrane (rBM) (Fig. 2a), similar to 3D rBM invasion[22]. Moving glioma cells retained connections with 3 to 5 neighboring cells while generating speeds of 120–140 μm/day (Extended Data Fig. 3a), as in sheet migration in monolayer culture[19,23].

To replicate diffuse infiltration into brain parenchyma in organotypic culture providing structural brain-like complexity, we visualized glioma cell invasion along 40–50 μm-thick 3D scaffolds consisting of immortalized mouse astrocytes and astrocyte-derived interstitial matrix[21]. Similar to neuropil infiltration, E-98 and E-468 cells glioma cells formed invading networks by aligning along astrocyte processes with tip-like cell junctions to an average of 3 to 4 adjacent glioma cells, while complete detachment of individual cells occurred rarely (Fig. 2b; Extended Data Fig. 3b). The cell-to-cell distance, number of connecting filaments and the number of connected glioma cells across interstitial in vitro (Fig. 2c–f) were similar

to glioma networks in vivo (Fig. 1b–c; Extended Data Fig. 1b–d and [12]), indicating multicellular organization as default state during glioma growth and invasion.

The filamentous interactions between glioma cells are reminiscent of dendritic protrusions and interactions between neuronal cells and astrocytes[24,25]. The connectivity between neuronal cells is compromised by high actomyosin contractility under the control of RhoA/ROCK signaling[26,27]. We therefore tested whether limiting Rho/ROCK further supports glioma cell interactions and network dynamics. ROCK inhibition significantly enhanced filamentous intercellular connectivity and invasion efficiency of E-468 cells into astrocyte scaffolds (Fig. 2g, h). This indicates that the invasion activity of glioma cell networks is enhanced by limiting actomyosin contractility, similar to developing neuronal networks[24]. This differs from Rho functions in epithelial tumors where limiting RhoA/ROCK signaling reduces invasion and metastasis[28,29].

Epithelial collective invasion results from relatively long-lived AJs between cells[18], however the organization and stability of AJs in moving glioma networks is unclear. During invasion cell-cell junctions between glioma cells interconverted between epithelial-like and filamentous junctions, dependent on cell density. Linear junctions were prominent when cell density was high near the spheroid (Fig. 2a, b). Filamentous junctions formed when cell density was low, dynamically connecting more sparsely distributed moving cells towards the invasion front, revealed by 3D time-lapse microscopy (Fig. 2i, j; Supplementary Video 5). We next analyzed how cell movement and junction stability are balanced. Anterior, lateral and rear filaments formed, persisted for several (up to 10) hours and resolved while interacting cells translocated (Fig. 2k). Because multiple junctions were engaged simultaneously at any time point, with a steady-state number of 2 to 6 connections/cell (Fig. 2l), cell movement allowed the network to expand (Supplementary Video 5). Connected cells leading the network maintained an oscillatory stop-go pattern with an average speed of 10 to 12 μm/h (Fig. 2k), similar to the speed of moving glioma cells in the mouse brain (5–15 μm/h)[30].

This variability of junction organization was consistent between in vitro models, glioma cells in the mouse brain and in patient glioblastoma samples, with epithelial-like linear or filament-based focal AJs between neighbor cells containing F-actin, β-catenin and p120 catenin (Fig. 2m, n)[31]. Thus, dependent on cell density and environmental context, glioma cells maintain cohesive or network-based junctions and anatomically adaptive collective invasion, not unlike astrocyte precursors migrating collectively during retina development[32] and reactive astrocytes after wounding[16,17].

Synchronous Ca2+ oscillations between invading glioma cells

In morphogenesis and mature brain, astrocyte networks share calcium transients, which are implicated in glial growth and neuronal signaling[33]. Moving individualized glioma cells exhibit non-coordinated calcium transients[8], but depend upon calcium channel activity for invasion, whereas stable glioma networks exhibit calcium transients across multiple cells[12]. To test whether moving glioma cells coordinate intercellular signaling, intracellular calcium ($[Ca^{2++}]i$) levels were recorded during emigration from spheroids. Connected E-98 and E-468 cells produced $[Ca^{2++}]i$ oscillations originating in individual or multiple cells

(Extended Data Fig. 3c, d) followed by signal spreading across fields of up to 20 cells (Extended Data Fig. 3e; Supplementary Video 6, 7). As in astrocyte networks[34], multicellular calcium transients were compromised by the connexin channel inhibitor carbenoxolone (CBX) (Extended Data Fig. 3f; Supplementary Video 8). Thus, collectively migrating glioma cells retain adhesive cell-cell junctions and intercellular signaling, similar to stable glioma cells networks[12].

Glioma cell coupling by adherens junctions

To test whether glioma-cell connections are critical for tissue invasion, we mapped and disrupted mechanisms of cell-cell cooperation. In epithelial, mesenchymal and neuronal cells, AJs depend upon E- and N-cadherin-mediated mechanical and functional coupling[31,35]. E-98 and E-468 cells expressed multiple classical cadherins (Extended Data Fig. 2c) and additional homophilic adhesion molecules, including ALCAM and NCAM (Extended Data Fig. 4a). Downregulation of N-cadherin, β-catenin and p120-catenin by transient RNA interference (RNAi) disrupted cell-cell junctions and facilitated cell individualization, with negligible impact by additional downregulation of ALCAM and NCAM (Extended Data Fig. 5a–d). This identifies classical cadherins in maintaining AJs between glioma cells.

p120-catenin as gatekeeper of glioma cell cooperation

As non-redundant intracellular regulator of AJs formed by classical cadherins, p120-catenin (p120) is essential in sustaining cell-cell interaction[36]. p120 promotes and stabilizes dendritic intercellular junctions in neuronal cells[36,37] and supports cohesive sheet migration in astrocytes in vitro[19]. p120 is upregulated in clinical glioma samples (Extended Data Fig. 4b), present along filamentous structures and cell bodies of glioma cells in the diffuse invasion zone (Extended Data Fig. 4c), and the phosphorylation status of Y228 of p120 is positively correlated with the invasiveness of patient-derived glioblastoma cells in the mouse brain[38]. In addition, cadherin-associated protein/δ2-catenin, an endogenous p120 antagonist primarily expressed in cells with neuronal differentiation, is target of inactivating driver mutations in glioblastoma[3]. These correlative data point towards a role for AJs and p120 in glioma progression, yet with unclear mechanism. To test its role in glioma network organization and function, we stably downregulated p120 by shRNA. In both PDX cells, p120 downregulation using 4 independent RNA sequences (70–80% efficacy verified by immunofluorescence analysis, qPCR and Western blot analysis) impaired cell-cell interactions followed by cell individualization, limited cell cycle progression with diminished mitosis rate and geminin expression, and caused an either de-novo (E-98) or persisting severe growth deficit (E-468) (Extended Data Fig. 5e–l). Moreover, downregulation of p120 compromised the formation of multicellular glioma networks (Fig. 3a) and prevented cells from participating in multicellular calcium wave propagation (Fig. 3b; Supplementary Video 9).

To address how cell-cell junctions deregulation affected moving glioma networks, we recorded their migration in the 3D astrocyte scaffold assay. After p120 downregulation, filament-like cell-cell junctions were lost and poorly polarized single cells, albeit mobile, failed to persistently migrate outward (Fig. 3d–h; Supplementary Video 10). Whereas

migration speed was undiminished after p120 silencing (Fig. 3g), the persistence and propagation of cells away from the spheroid were impaired (Fig. 3e). This reveals a critical role of p120 in securing collective polarity and migration persistence in glioma networks, similar to astrocyte sheet migration[19].

We next tested whether p120 initiates dendritic contacts or rather stabilizes existing junctions to coordinate glioma networks. P120 catenin controls the RhoA/ROCK pathway and limits RhoA-dependent actomyosin contractility including the light chain of myosin 2 (MLC2)[39,40]. Limiting p120 expression increased intracellular phospho-MLC2 (pMLC2), and ROCK inhibitor Y-27632 reverted pMLC2 levels in shP120 cells to near-control level (Extended Data Fig. 5m, n). As in control cells, Y-27632 further increased the number of filamentous connections in shP120 cells (Fig. 4a, b; compare Fig. 2g, h); however, in $p120^{low}$ cells, ROCK inhibition failed to restore both network organization and invasion into astrocyte scaffolds (Fig. 4b).

To identify the p120 domains required for glioma network formation, we reconstituted cells with stably downregulated human p120 with lentivirally encoded mouse p120 catenin sequences, which are functional in human cells[41]: (1) wild type (wt)[41], (2) p120 with K401M substitution in armadillo II domain decreasing p120 binding to cadherins[36,41], and (3) p120 with 622–628 deletion in the RhoA binding site, which reduces p120 mediated inhibition of RhoA activity[40,41] (Fig. 4c, d). Consistent with their predicted functions, p120wt and p120Δ622–628, but not p120K401M, increased N-cadherin expression on the glioma cell surface (Fig. 4e), as described[36,40].

Restitution of p120wt and p120K401M containing the Rho-binding domain normalized excess pMLC2 levels together with gain of filamentous protrusions, whereas p120Δ622–628 lacking the Rho-binding domain retained increased pMLC levels, together with defective filamentous protrusions to neighboring cells (Extended Data Fig. 6a, b). Moreover, expression of p120wt and p120Δ622–628 but not p120K401M increased β-catenin levels in E-468/shP120 cells (Extended Data Fig. 6c, d), consistent with p120 inhibiting RhoA and stabilizing cadherins and β-catenin at the plasma membrane[36].

Multicellular network formation was rescued by expression of p120wt, which restituted the ability of glioma cells to protrude filaments of equal number and length, compared to non-targeted control cells, formed extensive multicellular invasive networks in both 2D and 3D rBM culture (Fig. 4f, h, arrowheads, g, i; Extended Data Fig. 6e), and increased invasion ability compared to shRNA cells in 3D rBM (Fig. 4j). p120K401M reinstalled protrusive filaments but failed to support cell-cell connections between adjacent cells, resulting in protrusively moving cells with increased invasion distance in 3D rBM culture (Fig. 4f, h, asterisks; g, i, j; Extended Data Fig. 6e). Reconstituting p120Δ622–628 supported neither filamentous protrusions nor filamentous cell-cell interactions, resulting in persistent collapse of the network and impaired ability to migrate collectively (Fig. 4f–j; Extended Data Fig. 6e). Thus, both actomyosin contractility and cell-cell adhesion are required to form and stabilize filamentous cell-cell interactions and secure effective collective migration of glioma cells.

Moving networks thus reflect a previously unappreciated, neuronal/astrocytic type of collective cell migration in complex environments which depends upon adaptive AJs of variable morphology and contact duration, which differ from more cohesively moving epithelia or co-attraction coordinating collectively moving neural crest cells[42,43].

P120-catenin dependent networks mediate diffuse brain infiltration

We next aimed to delineate whether glioma cell networks are indeed required for diffuse brain infiltration. Luciferase-expressing E-98 cells as well as non-luminescent E-468 cells were implanted into the mouse brain and the effect of p120 downregulation on tumor growth and brain infiltration was monitored for up to 4 weeks (Fig. 5a) and/or whole-brain reconstruction and volumetric analysis *post mortem* after 4 weeks (Fig. 5b; Supplementary Video 11). Multifocal control tumors developed reliably over weeks (Fig. 5a), however p120-deficient cells failed to establish large or multifocal lesions and lacked diffuse brain infiltration (Fig. 5c; Extended Data Fig. 7a). Both, diffuse interstitial and perivascular invasion were compromised (Fig. 5c, d; Extended Data Fig. 7a), indicating a general migration defect in vivo. Overall, the reduction of diseased brain parenchyma after p120 targeting in glioma cells was reduced by 90–98% (Fig. 5c). To detect whether networks were disrupted by p120 downregulation in vivo, we performed 3D high-resolution morphometry of large-field sections capturing both tumor center and invasion front of E-468 PDX tumors (Fig. 5d). In control lesions, both tumor center and invasion front were composed of glioma cell networks with filamentous cell-cell junctions at an average of 3–4 cell-cell contacts (Fig. 5e) and gradual decrease of connection density towards the outward edge (Fig. 5f). After p120 downregulation, individualized and poorly polarized cells were retained, which failed to form interstitially invasive networks (Fig. 5d–f; Extended Data Fig. 7a). Residual microlesions contained few clustered cells lacking p120-positive intercellular junctions (Extended Data Fig. 7b) or individualized cells with shortened filaments positioned along interstitial tracks (Fig. 5d, Extended Data Fig. 7a; Supplementary Video 12), as well as compromised cell cycle progression detected by low frequency of geminin-positive cells (Extended Data Fig. 7c). In line with defective brain infiltration, colonization of the spinal cord was lacking in E-98 cells upon follow-up for up to 4 weeks (Fig. 5a). Thus, diffuse glioma cell invasion in brain tissue depends on p120 availability, resulting in poorly invasive, marginalized microlesions.

P120 regulates neuronal morphogenesis and cell proliferation pathways in glioma cells

To map the putative signaling mechanisms by which AJs may support glioma progression, we performed next-generation RNA sequencing and gene ontology (GO) analysis. Differential response patterns in glioma cells expressing non-targeting or p120 shRNA were largely cell-type specific with unique sets of down- or up-regulated genes, however with a significant cluster common to both E-98 and E-468 cells (Extended Data Fig. 2b and Extended Data Fig. 8a). GO-term analysis of downregulated gene sets identified perturbation of neuronal development, differentiation and axonogenesis in both cell lines (Fig. 6a, Extended Data Fig. 8b, Supplementary Table 2). Deregulated ephrins, netrins, neurofascin and contactin-2, among other targets (Fig. 6a), are critically involved in cell-cell interactions, neuronal development and synaptic transmission[44], and GAP43 mediates radiation resistance response of glioma networks[12] (Fig. 6a, Supplementary Table 2). Moreover, cell

cycle related pathways were significantly deregulated in E-468 after p120 knock-down (Extended Data Fig. 8b, Supplementary Table 2). Thus, p120 is a critical upstream regulator of signaling pathways required for neuronal-like network features in glioma cells.

High p120-catenin expression correlates with poor clinical outcome

To validate the role of p120 in glioma progression in human disease, we generated a p120 downstream gene signature using two independent datasets from human gliomas[45,46]. Genes that were up- and down-regulated after p120 downregulation in E-98 cells were directionally weighed-matched with gene expression data of clinical samples. The p120 signature significantly matched with signatures of genes involved in cell migration and extracellular matrix remodeling (Extended Data Fig. 8c), using the list of scanned 3875 Broad curated gene signatures. When stratified for p120 expression, overall survival of glioma patients was significantly prolonged in the subgroup with low p120 level (Fig. 6b), and a trend to accelerated progression was confirmed in the mesenchymal and classical, but not the proneural glioblastoma subtypes (Extended Data Fig. 8d). This result was in line with preferential upregulation of p120 mRNA in mesenchymal and classical, but not proneural, glioma subtypes (Extended Data Fig. 8e). Thus, in PDX models and clinical glioma samples, p120 regulated genes are associated with neuronal network, cell proliferation and migration functions and associated with glioma progression.

DISCUSSION

Multicellular networks which depend on filamentous protrusions connecting individual glioma cells have recently been identified as a major mechanism of glioma pathogenesis in the brain tissue[12,47]. Our findings identify p120 catenin as dynamic integrator of neuronal-like functions in invasive glioma cell networks. Rather than individualized, glioma cells migrate as a group, retain mechanocoupling, intercellular signaling and infiltrate the brain, similar to dynamic astrocytic or neuronal networks[24,48]. Glioma networks are adaptive, become cohesive when reaching the perivascular space, transiently cells individualize in outward regions (Extended Data Fig. 8f). The extensive intercellular connections imply that diffuse gliomas should be considered as a single functional operon, which as a whole sustains aggressive growth and survival ability[12,47] as well as brain infiltration.

AJs provide cell-cell adhesion and signaling for both neuronal-like network function in collective migration programs and growth, in potential reminiscence of certain epithelial tumors which rely upon p120 signaling for anchorage-independent growth, anoikis resistance and metastasis[49–51]. Our data establish p120 as a central gatekeeper of AJs[36] with oncogene-like functions in glioma, and deregulating p120-dependent signaling disables glioma aggressiveness. Similar to cell-cell cooperation drives epithelial tumor progression[52,53], targeting of AJs in glioma may dampen neoplastic growth and tissue infiltration programs congruently.

In contrast to epithelial collective invasion which depends upon continuous, cohesive cell-cell junctions in 2D and 3D environments[54], collective migration in glioma cells is remarkably adaptive and tissue-context dependent. While epithelial-like collective migration with linear cell-cell junctions, as used by glioma cells in the perivascular niche, is well-

established in epithelial embryonic and cancer models[18,55], glioma multicellular network migration combines neuronal network plasticity with transient cell-cell interactions in dynamic crest cells during morphogenesis[56,57]. Thus, despite their morphological adaptability, moving glioma networks retain mechanical and chemical coupling between cells and fulfill key criteria of collective invasion[18].

Molecular profiling after p120 downregulation indicates its role upstream of neurofascin, contactin 2, ankyrin G, MAP1B, doublecortin, GAP43 and other molecules (Fig. 7a; Supplementary Table 2), which regulate neuronal network formation[24,58,59]. AJs further mediate collective durotaxis of epithelial monolayers by mechanical coupling across multiple cell bodies, which strongly improves collective persistence towards stiffer substrate, compared to individually-moving cells[20]. AJs thus mediate morphogenesis-like multicellular front-rear polarity in glioma cell networks. P120 modulates the activity of Rho GTPases, which control the polarity of collective invasion and axonal growth[26,27,39,60,61]. By diminishing RhoA and engaging Rac1, p120 promotes extension of protrusions in neuronal cells[37,62]. Phosphorylation of p120 at Y228, which correlates with the invasiveness of glioblastoma cells in mouse brain[38], is required to limit RhoA[63]. However, in 3D invasion culture ROCK inhibition or expressing p120 with defective catenin-binding domain failed to rescue network invasion after p120 downregulation. This indicates that both, intact filament formation and adhesive strengthening of AJs are required for collective behaviors. Additional functions of p120 reside in its translocation to the nucleus and transcription regulation of genes implicated in neuronal differentiation via the transcriptional regulators KAISO, REST and GLIS2[64]. These effectors, which antagonize β-catenin/TCF/LEF transcriptional activity and modulate Wnt signaling pathways in axonal guidance and cell proliferation[39,64,65], may support glioma networks.

In conclusion, mechanical and signaling functions of p120-catenin are indispensable for maintaining neurogenesis programs in glioma cell networks, implicating AJs as key regulators of collective brain infiltration in glioma. Targeting of AJs or their downstream effectors may offer yet unappreciated strategies to overcome diffuse brain infiltration and fatal outcome.

Methods

Antibodies and reagents

The following antibodies were used for immunolabeling: anti-human IDH1 R132H (DIA-H09, mouse monoclonal, clone H09, Dianova; 1:20); anti-bovine GFAP (ab4674, chicken polyclonal, Abcam; 1:1000); anti-human myelin basic protein (M3821, rabbit polyclonal, Sigma-Aldrich; 1:200); anti-human nestin (MAB5326, mouse monoclonal, clone 10C2, human specific, Millipore; 1:200); anti-human nestin (ABD69, rabbit polyclonal, human specific, Millipore; 1:500); anti-human vimentin (ab24525, chicken polyclonal, Abcam; 1:400); anti-human vimentin (MA5–16409, rabbit monoclonal, SP20 clone, human specific, ThermoFisher Scientific; 1:300); anti-human tubulin (ab6046, rabbit polyclonal, Abcam; 1:200); anti-mouse p120 catenin (610134, mouse monoclonal, clone 98/pp120, BD Biosciences; 1:200); anti-human p120 catenin (ab32095, rabbit, clone YE372, human specific, Abcam; 1:200); anti mouse β-catenin (610153, mouse monoclonal, clone 14/beta-

catenin, BD Biosciences; 1:100); anti-human β-catenin (ab6302, rabbit polyclonal, Abcam; 1:1000); anti-mouse N-cadherin (C3865, mouse monoclonal, clone GC-4, Sigma-Aldrich; 1:200); anti-human ALCAM (559260, mouse monoclonal, clone 3A6, BD Biosciences; 1:50); anti-human NCAM (559043, mouse monoclonal, clone NCAM16.2, BD Biosciences; 1:100); anti-human geminin (PA5–30612, rabbit polyclonal, ThermoFisher Scientific; 1:500); anti-human phospho-(Ser 19)-myosin light chain 2 (3671, rabbit polyclonal, Cell Signaling Technologies; 1:100); anti-human phospho-(Ser 19)-myosin light chain 2 (3675, mouse polyclonal, Cell Signaling Technologies; 1:200); anti-mouse CD31 (DIA-310, rat monoclonal, clone SZ31, Dianova; 1:20); anti-mouse laminin (MA5–14657, rat monoclonal, clone LT3, ThermoFisher Scientific; 1:100); anti-human GAPDH 442 (2118, rabbit monoclonal, 14C10 clone, Cell Signaling Technologies; 1:10000).

Cell lines and culture

Human glioblastoma U-251MG cells (kind gift from Dr Joost Schalkwijk, Dept. of Dermatology, Radboudumc, Nijmegen, The Netherlands). Human glioblastoma E-98 and E-468 cells were maintained as patient-derived xenografts by serial intradermal (E-98) and intracerebral (E-468) inoculation without in vitro culture[14]. The study is compliant with all relevant ethical regulations regarding research involving human participants. The identity of U-251 cells was verified by short tandem repeat (STR) DNA profiling (IDEXX BioResearch). The STR DNA profile of E-98 cells, as published earlier[66], was confirmed and the profile of E-468 cells was generated for the first time (IDEXX BioResearch), as follows: AMEL, X; CSF1PO, 11, 12; D13S317, 10, 11; D16S539, 11, 12; D5S818, 12; D7S820, 8, 11; TH01, 9, 9.3; TPOX, 8, 10; vWA, 14, 17. The STR DNA profiles of E-98 and E-468 cells did not match any other reported profile in the DSMZ STR database (Leibniz Institute DSMZ, German Collection of Microorganisms and Cell Cultures GmbH). No mammalian interspecies or mycoplasma contamination was detected. E-468 cells were freshly isolated from mouse brain 8–10 days prior each transduction to minimize adaptation to in vitro culture, underwent showed very low baseline proliferation. A subline of E-98 cells was propagated in vitro in flasks for up to passage 35. For in vivo monitoring, E-98-Fluc-mCherry was generated by lentiviral transduction using firefly luciferase (Fluc) and mCherry construct (CSCW-Fluc-mCherry), as described[67,68]. To generate Lifeact-eGFP cells, pLentiCMV-MCS-Lifeact-eGFP vector (kind gift of Dr. Olivier Destaing, Institute Albert Bonniot, Grenoble, France) was introduced in E-98 and E-468 cells. Glioma cells were maintained in neurobasal medium (Invitrogen) supplemented with human EGF (20 ng/ml), human bFGF (20 ng/ml), B27 Supplement (1:50), L-glutamine (2 mM) (all from Invitrogen), heparin (2 μg/ml, Sigma), penicillin (100 U/ml) and streptomycin (100 μg/ml; both PAA). Cells were cultured either as 2D culture on flasks coated with growth factor-reduced reconstituted basement membrane (rBM) (Matrigel, Corning; 30 μg/ml in PBS, overnight at 4^{o}C) or as neurobasal spheroids. Accutase digestion (10 min, 400–600 units/ml; Sigma) was used for cell detachment and dissociation of the spheroids. E-98 cells were cultured at a minimum for 1 month in neurobasal media with regular change of media before their use for migration assays, lentiviral transduction or brain implantation. Primary mouse astrocytes immortalized with SV40 large T-antigen and additionally transformed with retrovirus pBabe puro H-Ras V12[69,70] were kindly provided by Amparo Acker-Palmer (Max Planck Institute for Brain Research Frankfurt, Germany). Murine astrocytes and, for selected

experiments, E-98 glioma cells were maintained in Dulbecco's Modified Eagle's Medium (DMEM; Invitrogen) supplemented with 10% fetal bovine serum (Sigma-Aldrich), penicillin (100 U/ml) and streptomycin (100 μg/ml; both PAA), L-glutamine (2 mM, Invitrogen) and sodium pyruvate (1mM, Invitrogen).

Confocal microscopy and quantitative image analysis

Confocal imaging was performed on an Olympus FV1000 microscope, using long working distance 20× NA 0.50 and 40× NA 0.80 objectives at step size of 2–3 μm. Large-field microscopy of tissue sections from murine and patient glioma lesions as well as multi-well in vitro culture of E-98 and E-468 cells on rBM was performed by automated high-content microscopy and image stitching (Leica DMI6000B). Imaris V.6.1.5 software (Bitplane) was used for 3D reconstruction of Z-stacks. For quantitative image analysis, operator-assisted image segmentation of 3D stacks and analysis were performed using Fiji analysis software (V.1.49g) for the following parameters: number of nestin-, vimentin- or IDH1 R132H-positive filaments extending per cell with connections to neighboring glioma cells; number of connected cells, as the number of neighboring glioma cells engaged with each glioma cell by IDH1 R132H, nestin- or vimentin-positive connecting filaments; the length of filamentous protrusions accounting for protrusions with a length >10 μm and width <7 μm; number of neighbors by epithelial-like junctions; distance between connecting glioma cell bodies as the direct line between 4',6-diamidino-2-phenylindole-(DAPI); organization of cell-cell junctions as the fluorescence intensity of cell-cell junction and filament markers along the intercellular junction line; migration speed, as the distance of either leading invasion edge or all cells from the spheroid margin.

Time-lapse confocal microscopy of Lifeact/eGFP expressing E-98 and E-468 cells was performed on a Leica-SP8 SMD confocal scanner equipped with high-sensitivity HyD detectors using 0.05 mW for excitation (488nm). Multicellular glioma cell spheroids were overlaid on non-fluorescent astrocyte scaffolds (day 2) and 3D stacks comprising the entire volume of the invasion zone were recorded every 20–25 min. The position of the cell body (centroid) for each cell was recorded manually for every frame using the maximum intensity projection to calculate speed for each step and confinement ratio (distance from start to end-point divided by total length of the path for an observation period of 10 to 13 hours). The number of cell-cell connections/cell during migration was obtained from individual slices to exclude false-positive projections.

Transient and stable downregulation of protein expression

Transient downregulation of adherens junction proteins and adhesion receptors was obtained for monolayer cultures on growth factor-reduced rBM using specific or matched non-targeting SMART-pool siRNAs (Dharmacon). For stable downregulation of p120 with lentiviral particles pLKO.1 (MISSION shRNA, Sigma-Aldrich), the following sequences were used:

Non-target shRNA, non- human or mouse shRNA (CCGG**CAACAAGATGAAGAGCACCAA**CTCGAG**TTGGTGCTCTTCATCTTGTTG**TTTTTG);

CTNND1 shRNA, TRCN0000122988 (CCGG**CTCCCAATGTTGCCAACAATA**CTCGAG**TATTGTTGGCAACATTGGGAG**TTTTTG);

CTNND1 shRNA, TRCN0000344830 (CCGG**ACTACCCTCCTGATGGTTATA**CTCGAG**TATAACCATCAGGAGGGTAG**TTTTTTG);

CTNND1 shRNA, TRCN0000344770 (CCGG**GCTTCGAAAGGCTCGTGATAT**CTCGAG**ATATCACGAGCCTTTCGAAGC**TTTTTG);

CTNND1 shRNA, TRCN0000333514 (CCGG**CGCCACTATGAAGATGGTTAT**CTCGAG**ATAACCATCTTCATAGTGGCG**TTTTTG).

After lentiviral transduction E-98 cells were propagated in neurobasal media using flasks coated with growth factor reduced rBM. The stability of p120 downregulation over consecutive cell passaging was verified by Western blot and PCR analysis. For transduction of patient-derived E-468 xenograft cells, intracranial tumors were isolated from mice, suspended, cultured (8–10 days) in neurobasal media on growth factor reduced rBM-coated flasks and transfected with lentiviruses. For in vitro and in vivo assays, cells were used after 8 day-culture after transduction in neurobasal media without subculturing. Efficiency of downregulation was verified by quantitative PCR and Western blot.

P120 catenin constructs

Three eGFP-tagged p120 catenin (mouse isoform 1A) pLV.CMV.IRES.puro constructs were a kind gift from Patrick Derksen (University Medical Center Utrecht, the Netherlands), and were functional in human cells as previously described[41]. The constructs encode the following p120 amino acid sequences: (1) wild type p120, (2) with K401M substitution decreasing p120 binding to cadherins[36], and (3) with 622–628 deletion in RhoA binding domain, which reduces p120 catenin mediated inhibition of RhoA activity[40]. Lentiviral particles were prepared for p120 constructs using ViraPower (Lentiviral Packaging Mix; Thermo Fisher Scientific). E-468 cells were transduced with lentiviral particles encoding murine p120 variants, selected with puromycin (3 μg/ml) after 3 days, and 1 day later transduced with human p120 shRNA lentiviral particles (MISSION shRNA, Sigma-Aldrich; sequence TRCN0000122988). The human specific p120 shRNA sequence does not match any sequences in mouse p120 catenin constructs based on RNA alignments (BLAST, NCBI). After secondary transduction, cells were maintained in a 96-well plate (Greiner Bio One, PS, F-bottom, μClear, Black, CELLSTAR) coated with growth factor-reduced rBM (Matrigel, Corning; 30 μg/ml in PBS, overnight at 4°C) for 5 days, followed by fixation (4% PFA). This sequence of lentiviral transductions in E-468 cells, in which overexpression of mouse p120 constructs preceded the downregulation of endogenous p120 by human-specific shRNA was required to minimize a consistently high rate of cell loss, including by adhesion deficiency and cell death after p120 downregulation under non-rescue conditions.

3D reconstruction of glioma lesions

Paraffinized clinical samples from glioma patients were obtained from the archives of the Department of Pathology, Radboud University Medical Center, Nijmegen. Samples included lower grade astrocytomas (LGA), anaplastic oligodendroglioma (with the characteristic complete deletion of chromosome arms 1p and 19q) and glioblastomas with wild-type and mutant isocitrate dehydrogenase 1 ($IDH1^{R132H}$) (Supplementary Table 1). The study is compliant with all relevant ethical regulations regarding research involving human participants. Informed patient consent and ethical committee approval for the use of (archival) brain tissue was obtained and the material was used in a manner compliant with the Declaration of Helsinki. Slices of 100 μm thickness were obtained by microtome slicing (HM 340E, Thermo Scientific Microm), deparaffinized (100% xylene), gradually rehydratated (sequential 100, 96, 70, 50% v/v ethanol/water), heated for antigen retrieval (98ºC, 15 min in Tris-EDTA, pH 9.0), incubated with blocking solution (0.05% Tween-20 and 1% bovine serum albumin in PBS) and stained with antibodies. Likewise, 200 μm thick sections from glioblastoma xenografts in mouse brain were obtained after fixation (4 % PFA, 20h) using vibratome slicing (Leica, VT1000s). To reach saturated antibody conditions and efficient washing in the 3D sample, incubation periods with primary and secondary antibodies and each washing step (0.05% tween-20/PBS; 0.05% NaN_3) were 8–24h at room temperature. Glioma cell populations in LGA and in glioblastoma with mutant IDH1 were identified by positivity for the IDH1 R132H mutation colocalized with nestin in the majority of cells. In glioblastoma with wild type IDH1 R132H, the presence of nestin in the absence of neuronal marker MBP was used to identify glioma cells[71].

Generation of glioma cell spheroids

Spheroids from E-98 and E-468 cells used in short-term migration assays were generated using the hanging drop method[72]. Cells were cultured in neurobasal media (Invitrogen) supplemented with human EGF (20 ng/ml), human bFGF (20 ng/ml), B27 Supplement (1:50), L-glutamine (2 mM) (all from Invitrogen), heparin (2 μg/ml, Sigma), penicillin (100 U/ml) and streptomycin (100 μg/ml; both PAA), to subconfluency, detached with accutase (400–600 units/ml; Sigma-Aldrich) washed with PBS, suspended in medium/ methylcellulose (0.12 – 0.24 %; Sigma-Aldrich) and maintained as hanging droplets (25 μL) containing 2000 (E-98) or 1000 (E-468) cells for 24 or 48 h.

Reconstituted basement membrane interface invasion assay

Glioma cell spheroids were placed on 96-well plates (Greiner Bio One, PS, F-bottom, μClear, Black, CELLSTAR) coated with growth factor-reduced rBM and, after initial attachment (3h), overlaid with 3D rBM (Matrigel, Corning; 5 mg/ml) as described[21]. After matrix polymerization, cultures were overlaid with neurobasal media, incubated for radial emigration (1–3d), fixed and stained for 3D confocal reconstruction and quantitative image analysis as described[21].

Astrocyte invasion assay

To generate 3D scaffolds, immortalized murine astrocytes were detached from subconfluent culture (1 mM EDTA /0.075% trypsin), transferred to 96-well plates (Greiner Bio One, PS,

F-bottom, μClear, Black, CELLSTAR) (20,000 cells/well) coated with growth factor-reduced rBM as described[21]. For invasion culture, 2–3 glioma cell spheroids/well were placed on top of consolidated astrocyte scaffolds (2 days), incubated for 2 additional days, fixed (4% PFA), stained and quantified for invasion efficacy and patterns by 3D confocal microscopy.

Live-cell calcium imaging

Glioma cell spheroids after growth in neurobasal media were placed on high-grade 96-well imaging plates (Greiner Bio One, PS, F-bottom, μClear, Black, CELLSTAR) coated with growth factor-reduced rBM (Matrigel, Corning; 30 μg/ml in PBS, overnight at 4°C). After 3–5 days of emigration from spheroids, cells were loaded with Fura-2AM (2.5 μM, 40 min; Invitrogen), washed once with neurobasal medium (20 min) followed by washing twice with Krebs solution (5.5 mM KCl, 147 mM NaCl, 1.2 mM $MgCl_2$, 1.5 mM $CaCl_2$, 10 mM glucose, and 10 mM HEPES/NaOH, pH 7.4) prior to imaging. Gap junctional communication was inhibited by carbenoxolone (CBX) (50 μM; Sigma-Aldrich) in Krebs solution at least 30 min before imaging. Imaging was performed by automated epifluorescence microscopy (BD Pathway 855, BD Biosciences; 37°C, 5% CO_2) using excitation at 340/26 nm and 387/11 nm and emission detection at 435LP nm with a 1.75s sampling interval. Ratiometric 340/380 analysis was performed using Attovision software 1.6/855 (BD Bioscience) and post-processed for spatiotemporal mapping using Fiji. For visualization of calcium waves, the cell fraction was masked in the 380 nm channel (thresholding followed by median filtering, radius 2.0 pixels) to define the cell regions for 340/380 ratiometric analysis. Cell boundaries were manually defined.

Flow cytometry

For surface protein expression analysis cells were detached with EDTA (2 mM), washed with PBS, incubated with primary antibody (10 μg/mL in PBS), washed, incubated with secondary Alexa488 or 647 conjugated antibody (Thermo Fisher Scientific, 1:400) and analyzed by flow cytometry (FACSCalibur, BD Biosciences). The cells were gated based on forward scatter and propidium iodide negativity (Extended Data Fig. 4a and Extended Data Fig. 5a) to exclude unspecific fluorescence from the final signal intensities or based on forward scatter and GFP positivity for cells transduced with p120 constructs (Fig. 5e) using software FCS Express (version 3 Research Edition; De Novo Software, Los Angeles, CA) and FlowJo (version 9.7.6; FlowJo LLC).

Reverse transcription and real-time quantitative PCR (RT-qPCR)

p120 mRNA levels after shRNA knock-down were analyzed by RT-qPCR. cDNA was prepared from 500 ng RNA with the SuperScript Reverse Transcriptase II kit (Invitrogen) using random hexamer primers. RNases were inhibited using RNaseOUT (Invitrogen). Pre-designed KiCqStart primers that were pre-validated according to the Minimal Information for Publication of Quantitative Real-Time PCR Experiments (MIQE) guidelines (Sigma-Aldrich) and the following three p120 primer pairs were used:

Primer pair		Sequence
P120-1	Forward	AGCAATATGGGATCAAACAC
	Reverse	TAAATCTTCTGCATCAAGGG
P120-2	Forward	GGAGCTATGAAGACATGATTG
	Reverse	CAAGCTTGCTAAACTTCCTC
P120-3	Forward	TGTGGAGCTCTCAAGAATATC
	Reverse	CCGGTAATAACTTCAGTAAGG

RT-qPCR was performed using CFX96 Real-Time PCR Detection System on a C1000 Thermocycler (Bio-Rad) and analyzed using the Bio-Rad CFX Manager software (version 2.0). For RT-qPCR, forward and reverse primers were used at a final concentration of 400 nM in 1x iQ SYBR Green Supermix (BioRad). The thermocycling program was: 10 min at 95˚C to denature the cDNA, followed by 40 cycles of 15 s at 95˚C and 50 s at 60˚C, and another 95˚C denaturing step for 15 s prior to a melting curve sequence from 65˚C to 95˚C at 0.5˚C increments. The threshold cycles (Ct) were normalized on a pool of 5 reference genes (GAPDH, β-actin, PSMB3, CANX, HMBS). The identity of the amplicon was confirmed by melting curve data. Appropriate no-template and no-reverse transcriptase negative controls included in each RT-qPCR run confirmed negativity in all cases.

Next-generation RNA sequencing

The RNA expression profile of glioma cells after stable transfection with NT or p120 shRNA were analyzed by RNA sequencing. Cells were maintained in culture with neurobasal medium for at least 4 weeks (E-98) or for 8 days (E-468) after lentiviral transduction. Total RNA was extracted using the column-based RNeasy micro kit (Qiagen) and the integrity and quality of obtained RNA was evaluated using the Experion RNA HighSens Analysis Kit (Biorad; #7007105) on a 2100 Bioanalyzer platform (Agilent). For cDNA synthesis starting from 1–10 ng total RNA, SMARTer Ultra low Input RNA kit (Clontech) was used and processed according to the manufacture protocol. The transcribed cDNA was sheared into fragments of 200–600 bp using Diagenode Pico sonicater. Subsequently the library preparation for Next Generation Sequencing has been carried out according to the Illumina standard protocol using the KAPA Hyper prep kit (KAPA Biosystems).

Raw data was aligned to the human genome using GSNAP aligner[73] and aligned reads annotation and counting was performed using HTSeq-count[74]. Differential expression analysis was performed using the DESeq package in R[75]. The log2 of fold changes +−1.5 with p value < 0.05 and FDR < 0.05 were used as criteria to determine the significant deregulated genes in p120-knock down samples compared to their matched NT-shRNA samples. Gene ontology analysis was performed using DAVID (https://david.ncifcrf.gov) and the KEGG database (http://www.genome.jp/kegg/) was used for pathway analysis. Clustering analysis of datasets was performed using GENE-E (http://www.broadinstitute.org/cancer/software/GENE-E/). Gene set enrichment analysis was performed using GSEA[76,77]. Non-supervised clustering was performed using normalized

read counts table as input and the one minus Pearson correlation was used as metrics distance. RNA-seq data that support the findings of this study have been deposited in the Gene Expression Omnibus (GEO) under accession codes GSE73999.

Bio-informatic analysis of human samples

Human samples were analyzed using the online platform R2 (r2.amc.nl). For gene ontology (GO) analysis, p120 shRNA knockdown experiments in E-98 glioblastoma cells resulted in a list of up and downregulated genes from which a directional gene signature was generated, taking the amount of genes into account (i.e. a directional and weighed signature). Using this signature, samples present in the glioblastomas (Verhaak, TCGA 540 samples, ID2000–01-01)[45] and low- to high-grade glioma (French dataset, 284 samples including normal controls, GEO ID: gse16011)[46] datasets were scanned for their match to the signature as based on the expression values of these genes and displayed as z-value with positive match displayed in red and inverse match in blue color. Kaplan-Meier analysis was done using p120 expression levels as a determinant of disease outcome, using the significance scanner option to identify the most optimal expression cut-off level to provide the highest, Bonferroni corrected statistical significance. Reactive and dynamic GO term analysis was performed by correlating the E-98 derived p120 signature with 3875 curated gene sets as provided by the Broad Institute (www.broadinstitute.org/gsea), using the TCGA 540 glioblastoma dataset. Results were top-ranked according to the correlation coefficient.

Glioma growth and invasion in mouse brain

Female athymic Balb/C nu/nu mice (6–8 weeks old), were obtained from Charles River Laboratories, maintained under specific pathogen-free conditions at the central animal facility, Radboudumc, Nijmegen. The study is compliant with all relevant ethical regulations regarding animal research. Animal procedures were approved by the Animal Ethics Committee of the Radboud University, Nijmegen (RU-DEC 2013–251) and performed according to the guidelines of the Dutch Act on Animal Experimentation and the European FELASA protocol. E-98-Fluc-mCherry and unlabeled E-468 parental cells were cultured as spheroids in neurobasal media, enzymatically dissociated by accutase digestion, and intracranially implanted (5×10^5 cells in 20 μL PBS) by guided injection into the right parieto-occipital hemisphere of isofluorane-anesthetized mice 2 mm from the midline. E-98-Fluc-mCherry and unlabeled E-468 cells with control and p120 shRNA (sequence TRCN0000122988) were cultured for more than 4 weeks (E-98) or 8 days (E-468) after lentiviral transduction in neurobasal media on growth factor reduced rBM-coated flasks and intracranially implanted in 20 μL PBS per mouse − 0.4 or 0.8×10^5 of E-98 and 0.4 or 1.0×10^5 of E-468 cells. The extent of tumor growth and diffuse brain infiltration was quantified by whole-brain vibratome sectioning (200 μm thickness) followed by counterstaining to detect murine astrocytes by anti-GFAP pAb and glioma cells by human-specific anti-vimentin pAb. The extent of glioma infiltration was obtained by automated high-content microscopy (Leica DMI6000B) from whole-brain vibratome slices (200 μm thickness) followed by manual segmentation using the vimentin channel (Fiji). Quantitative image analysis from 3D confocal stacks (40x, NA 0.8) was performed to extract the frequency of geminin-positive cells, the number of cell-cell contacts per cell and the subcellular location of p120 in glioma cells using anti-human p120 mAb.

In vivo bioluminescence imaging

Fluc-E98/NTshRNA and Fluc-E98/p120 shRNA in mouse brain and spinal cord was monitored with IVIS Lumina imaging system (Caliber). Luciferine (200 μL; 15 mg/ml in PBS) was injected intraperitoneally in isofluorane-anesthetized mice and bioluminescence was detected in 10 min. Photon emission was normalized to photons per second per centimeter squared per steradian (p/s/cm2/sr).

Statistics and Reproducibility

Unless stated otherwise, all experiments were reproduced by at least 3 independent experiments. P-values were obtained using two-tailed Mann-Whitney test or one-way ANOVA Dunnett's multiple comparison test. The significance of the GO terms (RNA sequencing data) was calculated using one-tail Fisher Exact Probability test implemented in DAVID online database. Further details about the statistics are stated in the Figure legends.

Data availability

RNA-seq data that support the findings of this study have been deposited in the Gene Expression Omnibus (GEO) under accession codes GSE73999. RNA expression data that support the findings of this study are available in the cBioportal (TCGA) and the GEO data repositories. The human glioblastoma analysis was first performed on the TCGA dataset, available as "Tumor Glioblastoma - TCGA- 540 - MAS 5.0 - u133a"[2] in the R2 database (R2.amc.nl), source data available at https://www.cbioportal.org/. The next analysis was performed on human glioblastomas data of the French dataset (gse16011), available as "Tumor Glioma - French - 284 – 540 - MAS 5.0 - u133p2"[46] in the R2 database [R2.amc.nl].

All other data supporting the findings of this study are available from the corresponding author on reasonable request.

Extended Data

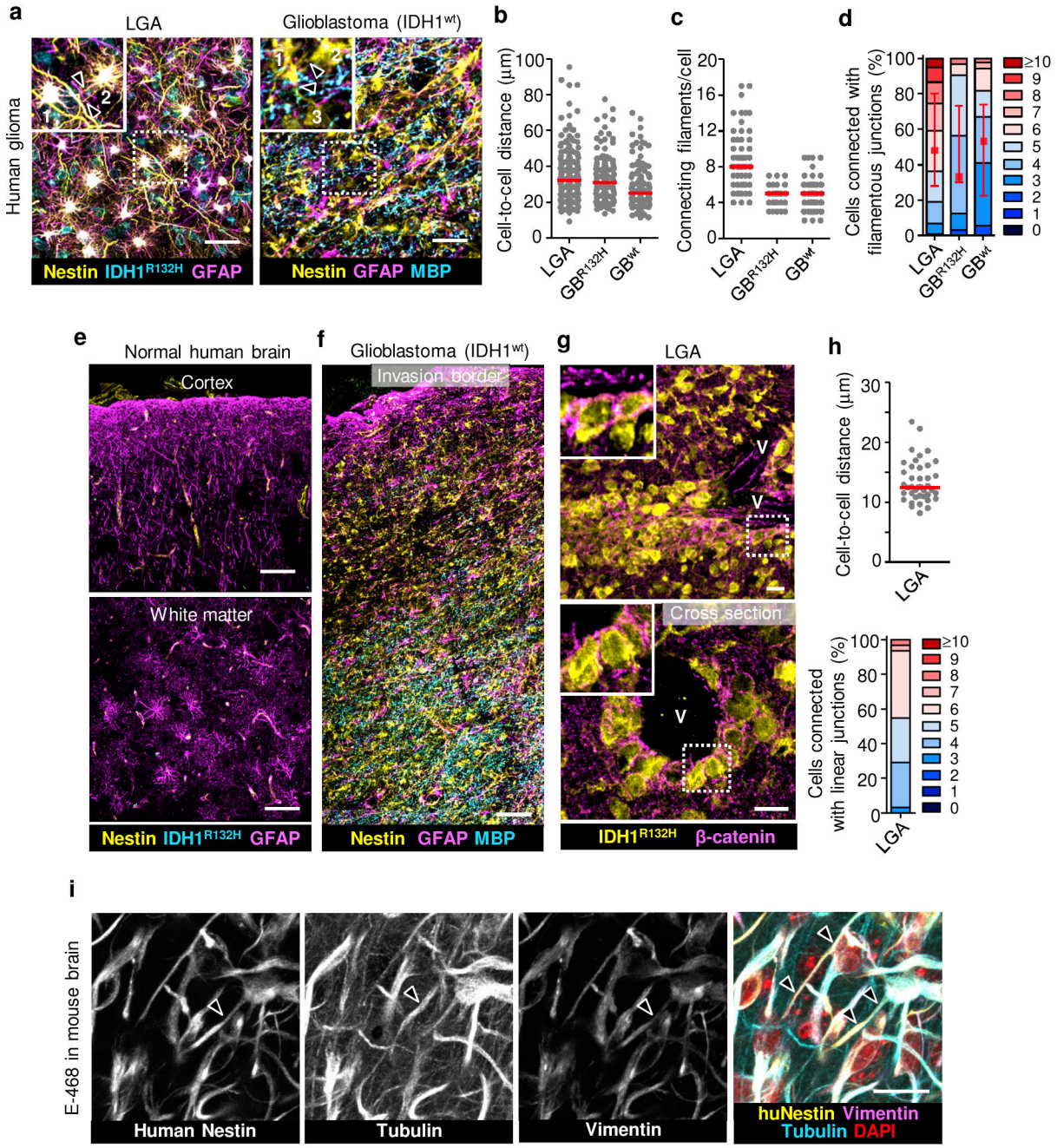

Extended Data Fig. 1. Identification of glioma cell networks and cohesive perivascular invasion zones in patient samples.

a-d, Morphological pattern and quantitative cell-cell junction analysis of glioma cell networks detected in 30 or 100 µm thick tissue slices. Samples included lower-grade astrocytoma with mutant IDH1 (LGA, grade II and III), glioblastoma with mutant (GB^{R132H}) and wild type IDH1 (GB^{wt}). Detailed information in Supplementary Table 1. Images represent the peritumor region of the lesions. Identification of glioma cells in LGA and GB^{R132H} via colocalization of $IDH1^{R132H}$ and nestin. In $IDH1^{R132H}$ negative glioblastoma, glioma cells are identified as nestin-positive but Myelin Basic Protein-(MBP)

negative networks. Similar results as in (a) were observed in brain samples from 8 (LGA) and 4 (GB^{wt}) patients. Data represent 28–58 (b), 7–28 (c) or 14–34 (d) cells per sample from 6 (LGA), 1 (GB^{R132H}) and 4 (GB^{wt}) patients. **e,** Tumor-free human brain cortex and adjacent white matter region lacking $IDH1^{R132H}$ and interstitial nestin signal, but contain GFAP-positive astrocytes in the parenchyma. **f,** Representative large-field overview used for selecting region for high-resolution imaging. Nestin-positive but myelin basic protein-(MBP-) negative glioma cell network in glioblastoma multiforme (GBM) sample intercalating with astrocyte (GFAP) and myelinated axonal (MBP) networks in tumor margin. **g,** Perivascular cohesive glioma cell layers aligning along large vessel, identified by longitudinal or cross-section lumen (V) in LGA sample. Inset, β-catenin-positive cell-cell junctions. **h,** Cell-cell proximity and number of directly neighboring cells during perivascular invasion (3D image analysis of LGA samples). Data represent 20 cells per sample from 2 LGA patients. **i,** Molecular topography of filamentous protrusions connecting glioma cells in patient-derived orthotopic E-468 xenograft. Identification of glioma cells using human-specific anti-nestin mAb. Arrowhead, nestin- and vimentin-positive filament, also containing microtubules. Similar results were observed in 3 mice. Scatter dot plots show the medians (red line) and values representing individual cells (b, c, h); in (d, h) values display relative fractions of connected glioma cells interacting with 0 up to 10 connected cells (boxes), median (red square), 25/75 percentiles (whiskers). Scale bars, 50 μm (a), 100 μm (e, f), 20 μm (i, g).

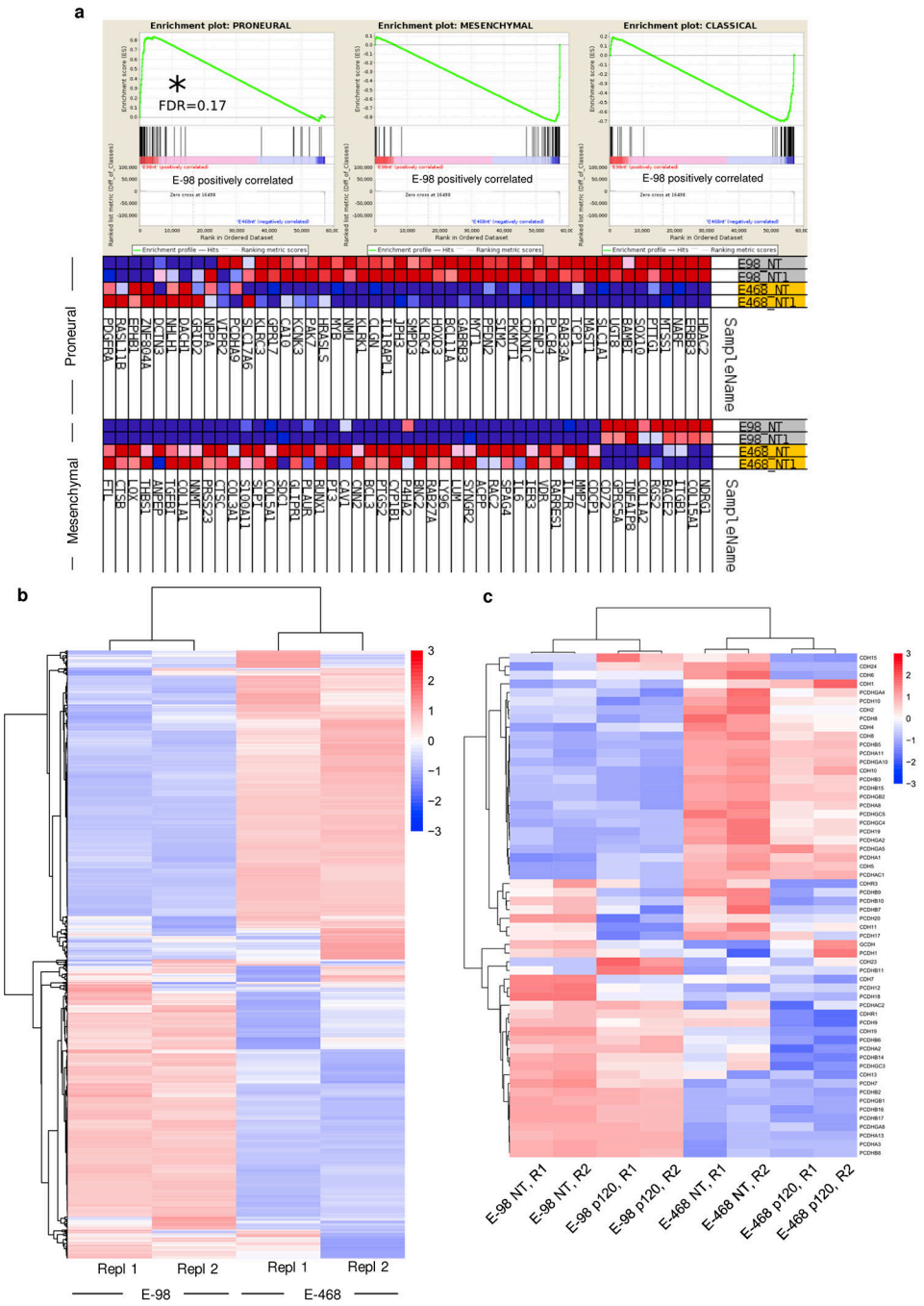

Extended Data Fig. 2. Subtype analysis and differential gene expression of E-98 and E-468 glioma cells.

a, Gene set enrichment analysis on non-targeting shRNA samples (from two independent RNA isolations per cell line) of E-98 (NT shRNA) and E-468 (NT shRNA) cell datasets using 3 glioblastoma subtype gene sets[11]. **b**, Hierarchical clustering and heatmap of mRNA expression of genes found to be deregulated after p120 knock-down (compare Supplementary Figure 8). Data represent the gene expression in cells after lentiviral transduction with non-targeting shRNA (from two independent RNA isolations per cell line).

c, Hierarchical clustering and heatmap of cadherin and protocadherin genes detected in at least one of the replicates. The Euclidean distance was used as metrics and the normalized expression level of genes used as input values and z-score values were used for visualizations.

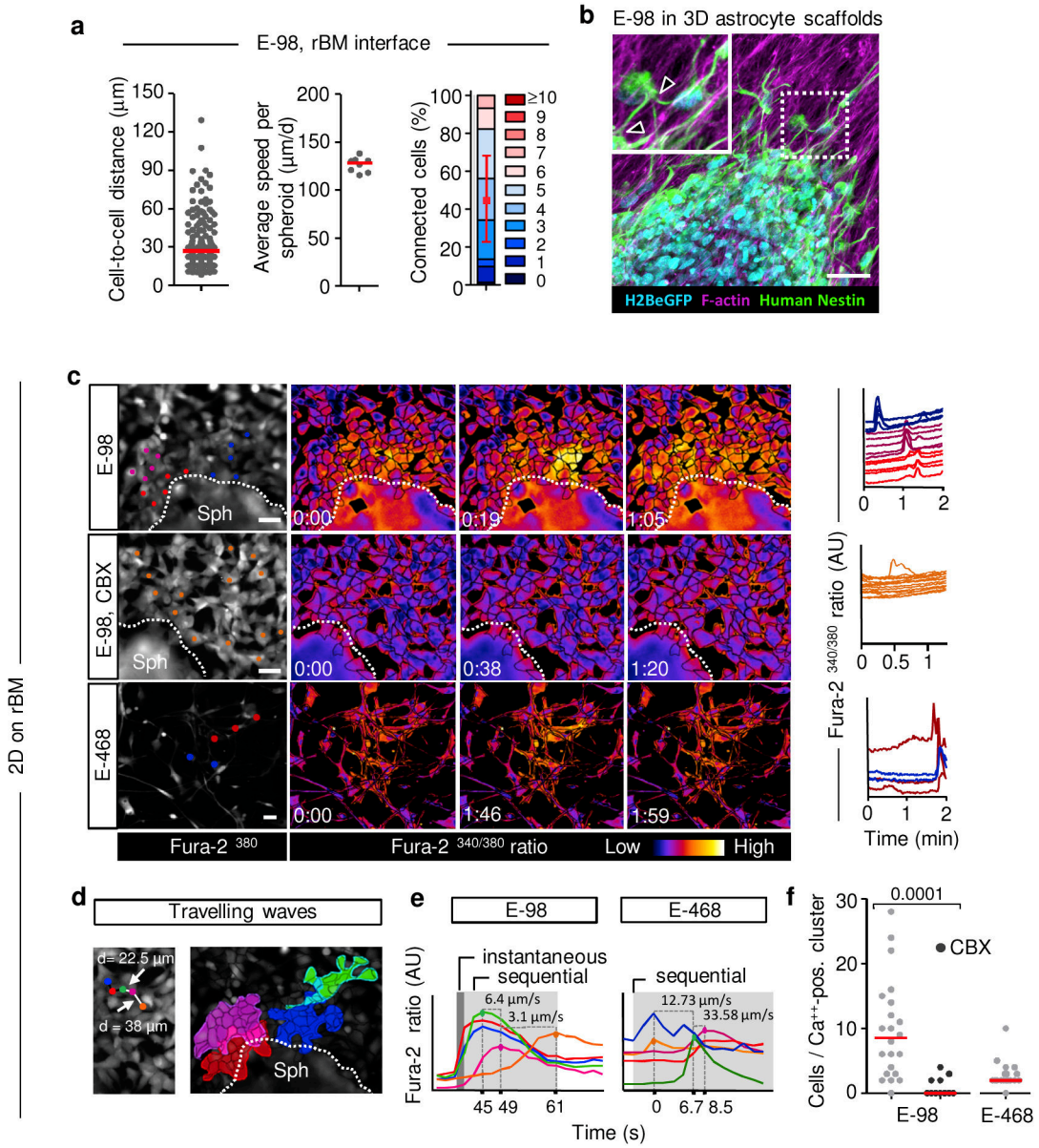

Extended Data Fig. 3. Variability of cell-cell interactions and functional coupling of glioma cells during migration.

a, Quantification of next-neighbor proximity, migration speed and cell-cell interactions in E-98 glioma cell invasion in reconstituted basement membrane (rBM) assay after 48 h of invasion culture. Data represent 272 cells (left panel), 8 spheroids (middle panel) or 73 cells (right panel) from two representative from 3 independent experiments. Scatter dot plots show the medians (red line) and values representing individual cells (left plot) or spheroids (middle plot); in the right graph values display relative fractions of connected glioma cells interacting with 0 up to 10 connected cells (boxes), median (red square), 25/75 percentiles (whiskers). **b,** Cell pattern of E-98 glioma invasion (48 h) from multicellular spheroid (Sph) into 3D astrocyte scaffolds. Arrowheads indicate filamentous cell contacts. Similar results were observed in 3 independent experiments. **c,** Functional cell-cell coupling in E-98 and

E-468 cells measured as intracellular calcium transients and inhibition of multicellular calcium transients in E-98 cells in the presence of carbenoxolone (CBX, 50 μM). Cell identification for ratiometric time-series (left panels) and derived calcium transients in neighboring cells (right panel). Dots, cells assessed for calcium transients displayed in the graphs. Sph, spheroid. Similar results were observed in 3 independent experiments. **d,** Near-instantaneous and sequential calcium transients in E-98 and E-468 cell clusters and networks. Example micrograph highlighting neighboring cells participating in calcium wave (left panel) and fields of connected cells recorded over 2 min (right image). **e,** Calcium waves and propagation speed (in brackets). The propagation speed in E-98 is consistent with the velocity of calcium waves between astrocytes (approx. 6 μm/s)[78].
Similar results were observed in 3 independent experiments. **f,** The number of cells in synchronized clusters of E-98 and E-468 cells. Data represent 22 (E-98), 11 (E-98, CBX) and 18 (E-468) cell clusters from 3 independent experiments. Scatter dot plot shows the medians (red line) and values representing individual cell clusters (dots). P values were obtained using two-tailed Mann-Whitney test. Scale bars, 50 μm.

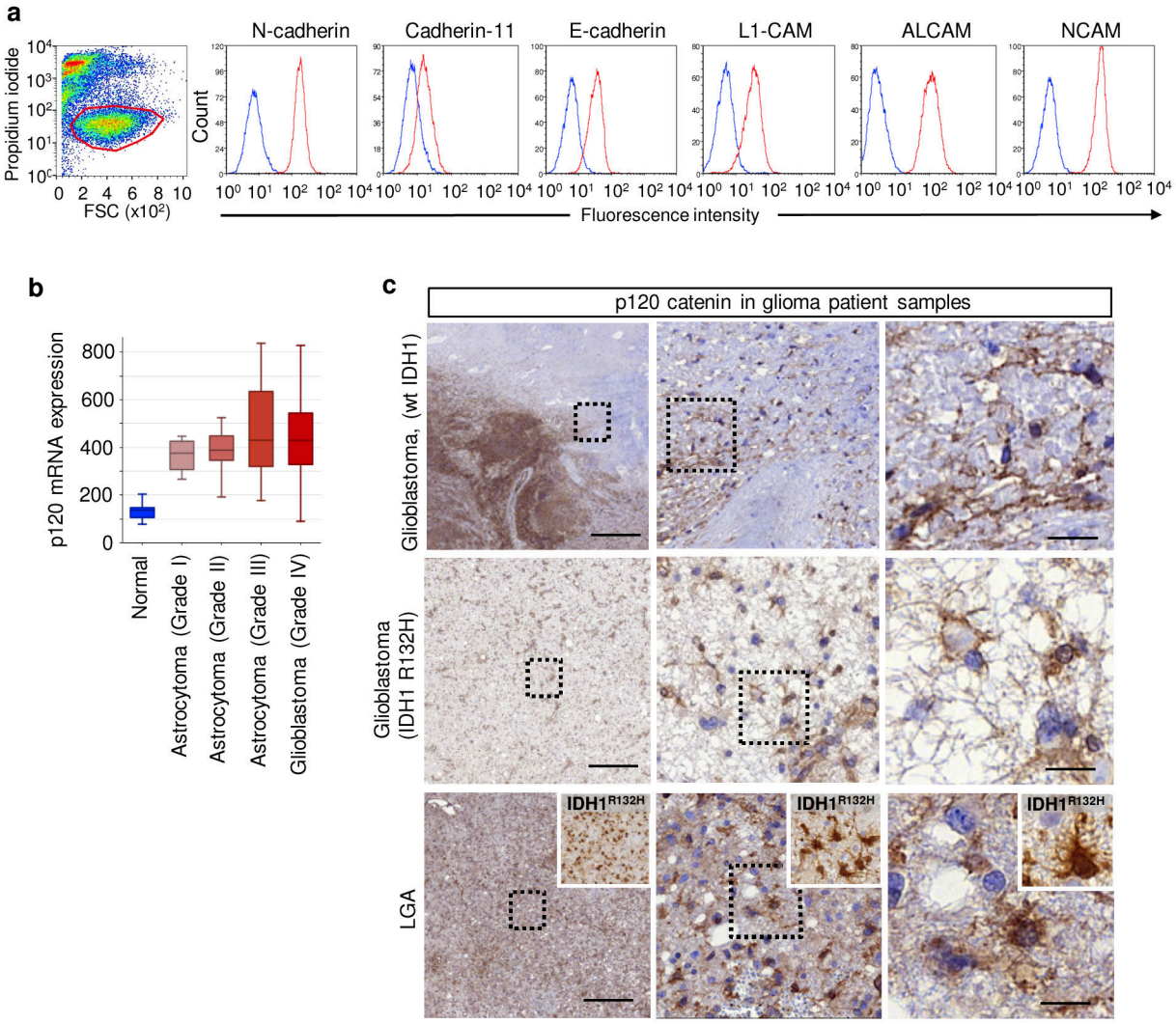

Extended Data Fig. 4. Expression and subcellular distribution of p120 and other cell-cell adhesion molecules in human glioma cells.

a, Surface expression of receptors implicated in cell-cell interactions in E-98 cells (FACS data). Similar results were observed in 2 independent experiments. **b,** Increased expression of p120 catenin in human gliomas of different grade. Data are derived from French dataset (MAS5.0-u133p2) comprising grade I-IV gliomas (n=284 patients)[46]. Expression reflects log level. Box plots display the median (black line), 25/75 percentiles (boxes) and maximum/minimum (whiskers) from 8 (normal brain), 8 (grade I), 13 (grade II), 16 (grade III) and 159 (grade IV) glioma patients. **c,** p120 (brown label in large panels) and $IDH1^{R132H}$ (insets) immunohistochemistry in glioblastomas and low grade astrocytoma (LGA) samples. P120 positivity in both tumor core and diffuse brain infiltration region. $IDH1^{R132H}$ positivity in grade III glioma sample was used to confirm glioma cell origin. Similar results were observed in 2 independent immunohistochemistry staining of samples from 2 (LGA), 1 (GB^{R132H}) and 2 (GB^{wt}) patients. Scale bars, 500 μm (overviews) and 20 μm (details).

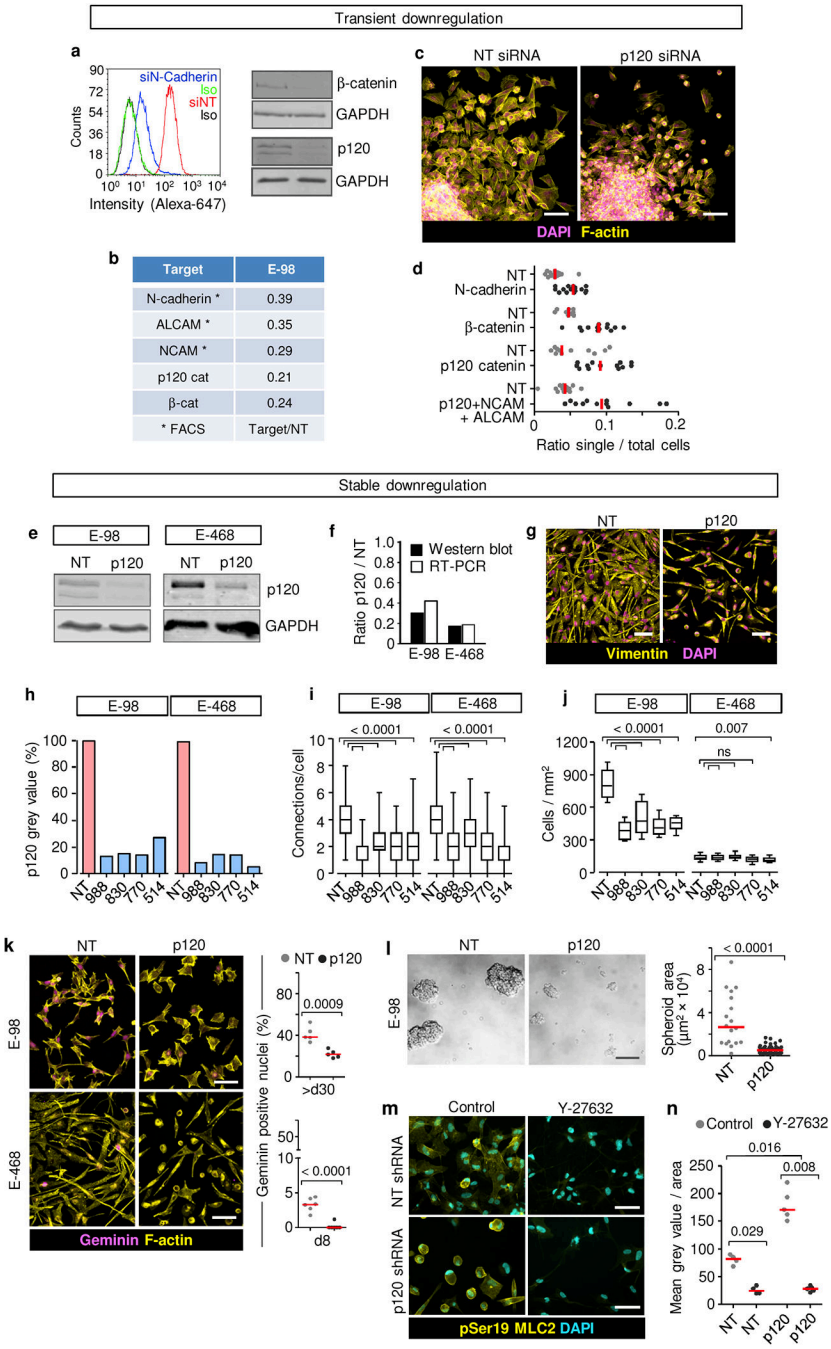

Extended Data Fig. 5. Molecular targeting of glioma cell-cell interaction and collective invasion in vitro.

a-d, Transient downregulation of candidate proteins involved in cell-cell junction stability of E-98 cells. (a) Relative protein levels detected by Western blot (total proteins) or flow cytometry (surface receptors) after transient downregulation using SMARTpool siRNA. Similar results were observed in 2 independent siRNA transfections. Unmodified scan of the Western-blot is provided in Source data. (b) Numbers in the table express the ratio between p120 and non-targeting (NT) siRNA. (c) Morphology and (d) quantification of single-cell fraction during radial migration of E-98 glioma cells from spheroids on rBM-coated surface

after single- or triple interference with cell-cell junction proteins. Similar results were observed in 3 independent siRNA transfections. Data in (d) represent 9–15 spheroids per condition from 3 independent siRNA transfections. Scatter dot plots show individual spheroids and medians (red line). **e-l,** Quality control and functional consequences of stable downregulation of p120 in glioma cells. **e-g,** Extent of downregulation of p120 protein (e, f) and p120 mRNA (f) and persistence of vimentin expression in E-468 cells (g). Similar results were observed in 2 (e, f) or 3 (g) independent shRNA lentiviral transductions. Unmodified scan of the Western-blot (e) is provided in Source data. Immunostaining of human vimentin was used for the detection of glioma cells in the mouse brain. **h-j,** Effect of four independent shRNA sequences on p120 catenin protein levels detected by immunofluorescence (h), the number of cell-contacts between neighboring cells (i) and cell density as measure for growth (j). Data represent 313–2353 (h), 196–228 cells (i) and 669–3153 (j) cells per shRNA sequence per cell line from 3 independent shRNA lentiviral transductions. Values in (h) show the means. Values in (j) represent the means of cell number per area (650×486 μm). Box plots in (i, j) display the median (black line), 25/75 percentiles (boxes) and maximum/minimum (whiskers). P values, two-tailed Mann-Whitney test. Based on efficacy of p120 downregulation and representativity, sequence TRCN0000122988 was used for further in vitro and in vivo experiments. **k,** Cells in S/G2/M phase detected by geminin staining >30 (E-98) or 8 days (E-468) after transduction with p120 shRNA. Data represent 238–475 cells in 5–6 areas (650×486 μm) per condition in one representative of 3 independent shRNA transductions. P values, two-tailed Mann-Whitney test. In contrast to E-98 cells which grew well in liquid culture before p120 downregulation, E-468 cells were derived directly from mouse brains and failed to grow in vitro. **l,** Reduced growth of E-98 cells in neurobasal spheroids after p120 downregulation. Data represent 18 (NT shRNA) and 53 (p120 shRNA) spheroids from one representative of 3 independent shRNA transductions. P values, two-tailed Mann-Whitney test. **m, n,** Myosin light-chain phosphorylation (ROCK target) after p120 downregulation in E-468 cells in the absence or presence of ROCK inhibitor Y-27632 (10 μM) detected by cell-based immunofluorescence. Data represent 84–171 cells from one representative of 3 independent shRNA transductions. P values, two-tailed Mann-Whitney test. Scatter dot plots show the medians (red line) and values representing individual spheroids (d, l) or areas (650×486 μm) in 96 well plates (k, n). Scale bars, 100 μm (c, g, k, m), 200 μm (l).

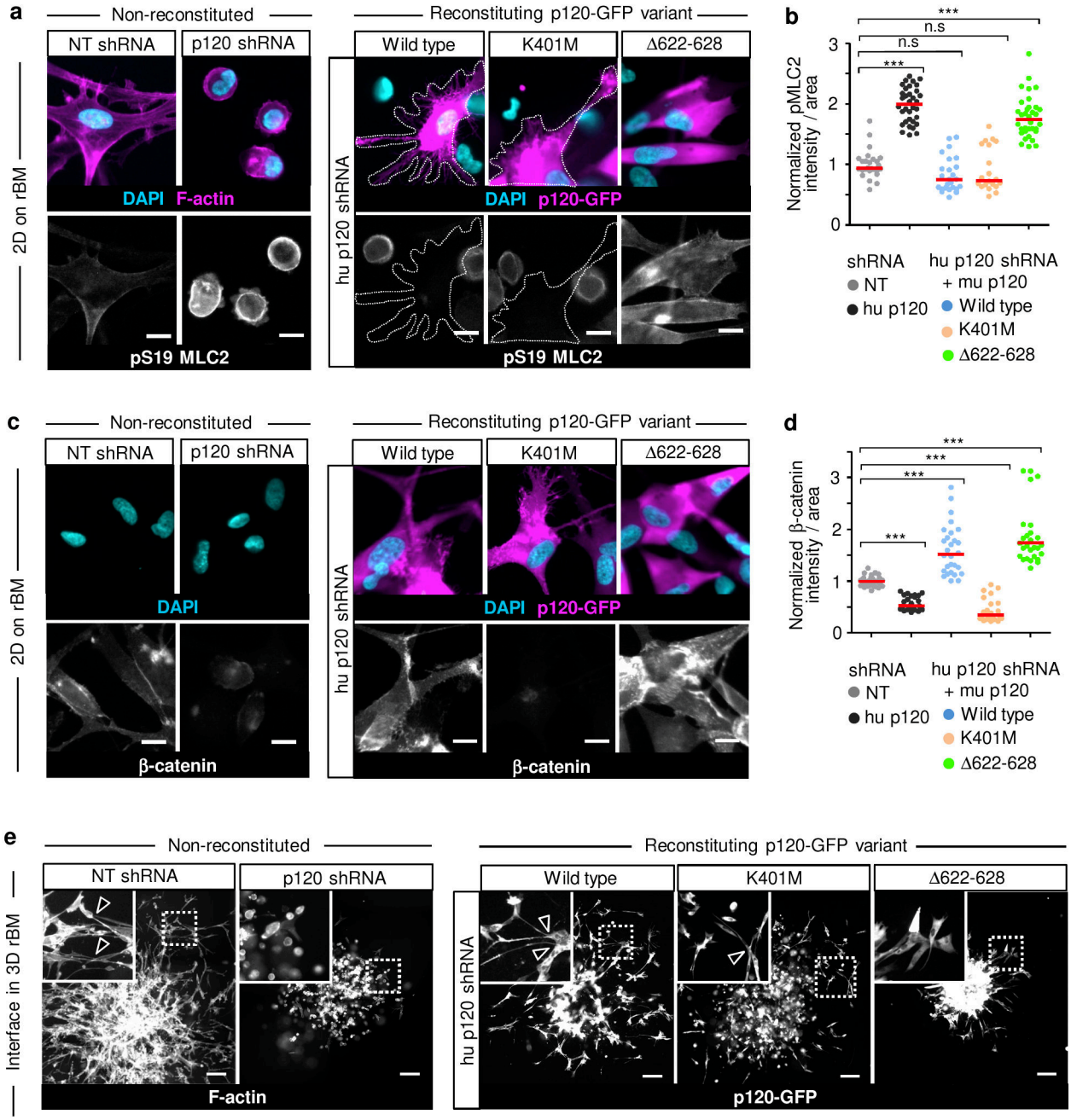

Extended Data Fig. 6. Myosin light-chain 2 phosphorylation and β-catenin expression in E-468 cells and radial invasion from spheroids after p120 downregulation and reexpression of p120 mutants.

a-d, Myosin light-chain 2 (Ser 19) phosphorylation (a, b) and β-catenin expression (c, d) during E-468 cell culture on rBM after transduction with non-targeting shRNA, human p120 shRNA or human p120 shRNA with additional transduction with mouse p120-eGFP constructs (indicated in Fig. 4c) encoding wild-type p120 catenin, p120 with K401M substitution and p120 with 622–628 deletion. Similar results as in (a, c) were observed in 3 independent shRNA lentiviral transductions. Mean intensity of phospho-Ser19-MLC2 (b) or β-catenin (d) immunofluorescence in p120 shRNA cells after re-expression of p120 catenin

constructs. Data in (b, d) represent the fluorescence intensity per imaging field (650×486 μm) covered by multiple cells from 20–34 (b) or 26–33 (d) fields per condition from 3 independent lentiviral transductions. Scatter dot plots in (b, d) show the normalized fluorescence intensity per area (650×486 μm) and medians (red line). P values, one-way ANOVA Dunnett's multiple comparison test. ***, P<0.0001. **e**, Overviews of migration and intercellular organization of E-468 cells invading from multicellular spheroids along 3D rBM interface after 3-day culture (described in Figure 2a). Similar results were observed in 2 independent shRNA transfections. E-468 cells were transduced with non-targeting or human p120 shRNA and additionally mouse p120-eGFP constructs encoding wild-type p120 catenin, p120 with K401M substitution and p120 with 622–628 deletion. Arrowheads indicate filamentous cell-cell contacts. Scale bars, 20 μm (a, c); 200 μm (e).

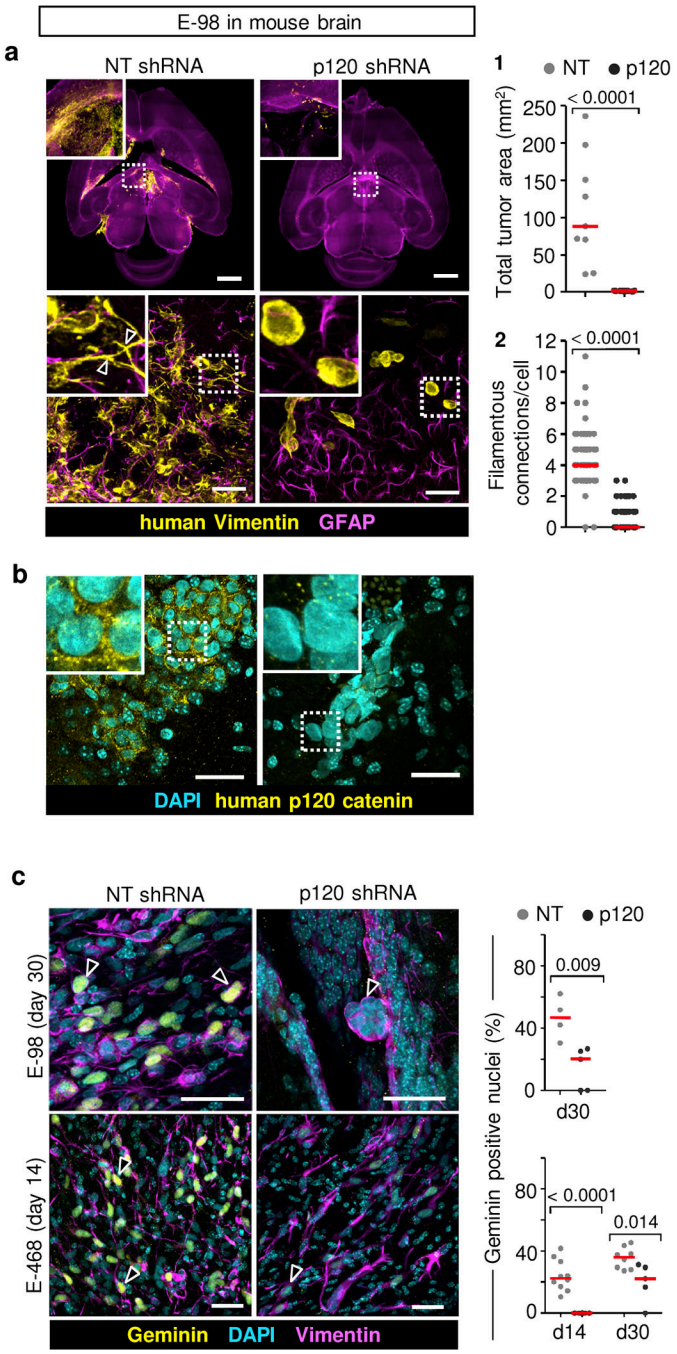

Extended Data Fig. 7. Inhibition of multicellular networks and diffuse infiltration into mouse brain after p120 downregulation.

a, Impaired tumor growth, loss of network formation and diffuse brain infiltration of E-98 cells after p120 downregulation. Overviews (upper panels) and zoom images (lower panels) from 200 μm thick brain slices. Arrowheads, filaments in multicellular networks of human vimentin-positive E-98 cells diffusely infiltrating the brain. Data represent 9 (NT shRNA) or 10 (p120 shRNA) mice from 2 independent experimental series (a1) and 49 cells (NT shRNA) or 89 (p120 shRNA) cells from two mice per condition (a2). P values, two-tailed

Mann-Whitney test. **b,** Persistent deficiency of p120 signal in vivo in p120 shRNA knock-down E-98 cells in 4 weeks after intracranial tumor implantation. Similar results were observed in two mice per condition. **c,** Sustained glioma growth deficit in vivo after p120 downregulation. Frequency of geminin-positive glioma cells after the indicated time of post-implantation in mouse brain. Data represent 42–201 (E-98) and 108–574 (E-478) cells from 4–5 (E-98) or 5–21 (E-468) imaging fields from two mice per condition. P values, two-tailed Mann-Whitney test. Scatter dot plots show the medians (red line) and values representing individual mice (a1), individual cells (a2) or imaged areas in brain slices (c). Scale bars, 2 mm (a, upper panels), 50 μm (a, lower panels; b, c).

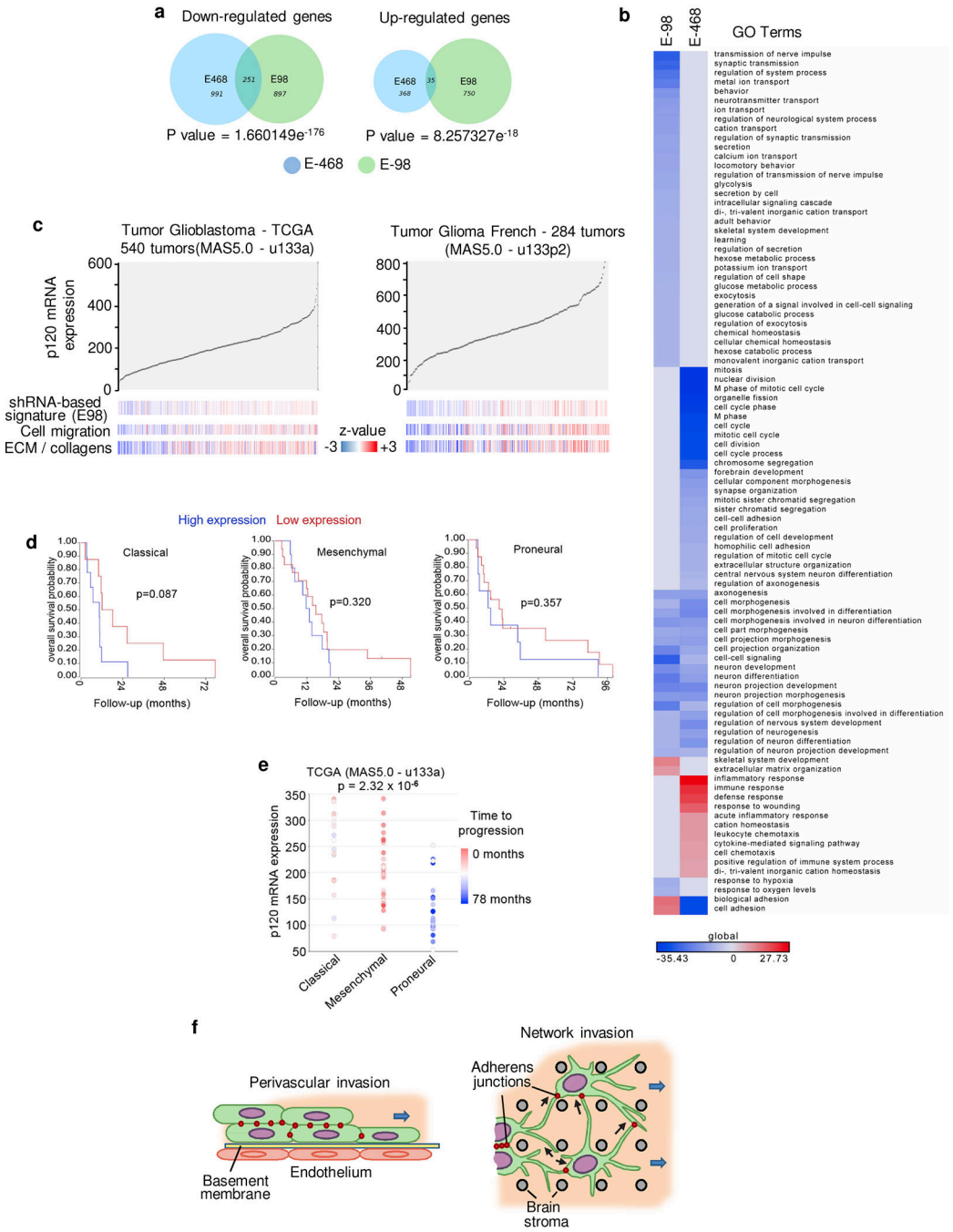

Extended Data Fig. 8. Gene expression regulation in glioma cells in response to downregulation of p120 and clinical relevance of p120 catenin in glioma patients.

a. Proportional Venn diagrams of total number of down- (n=1,148 and n=1,242) or upregulated (n=785 and n=403) genes in E-98 and E-468 cells respectively after p120 downregulation (*p* values are obtained using hypergeometric test). **b**, Ranked list heatmap of all relevant GO term biological functions resulting from gene ontology analysis of deregulated genes in each p120 knock-down cell lines. Absolute Log2 transformed Benjamini-Hochberg FDR values per each GO term were used as input in which the

upregulated terms were converted to a positive and the downregulated terms to a negative number in the color scale scoring. The annotation was carried out using the DAVID server and GO database and the FDR <= 10^{-3} was determined as cut off for selecting the relevance of the GO terms. To determine the significance of deregulation, log2-fold change of >1.5 for upregulation and < −1.5 for downregulation and two-sided test p value < 0.05 and FDR < 0.05 were used as cut offs. The gene ontology analysis was performed based on data obtained from two independent RNA isolations per condition (n=2). **c**, Gene enrichment analysis of the p120 signature in human glioma. Expression levels of p120 correlate to migration/ECM gene signatures. Ranked expression panels of p120 RNA expression as determined by MAS5.0 normalized u133a or u133p2 RNA expression arrays (Verhaak, TCGA 540 tumors, ID2000–01-01)[45] and low- to high-grade glioma (French 284 samples including normal controls, GEO ID: gse16011)[46], correlated to z-values of a migration signature[79]; n=540 and n=284 patients, respectively. (http://www.broadinstitute.org/gsea/msigdb/cards/WU_CELL_MIGRATION.html) and an ECM signature (Segal Stanford cancer modules, http://ai.stanford.edu/~erans/cancer/modules/module_47.html). **d**. Kaplan Meier survival curves of p120 mRNA expression within glioma subtypes. Trends show decreased survival in the $p120^{high}$ subgroup, but do not reach statistical significance due to low case numbers (proneural: n=24; mesenchymal: n=27; classical: n=17). P-values, two-tailed Mann Whitney test (raw, non-Bonferroni corrected). **e**, Expression of p120 mRNA in the three subtypes of glioblastoma, as defined by Verhaak et al[45] (TCGA dataset, MAS5.0 - u133a, 540 patients of which n=68 subtype classified patients are shown). The time to progressive disease is indicated as a heatmap value for each patient (red indicates immediate progressive disease; blue indicates delayed progressive disease). This shows that p120 is highly expressed in the classical and mesenchymal subgroups which have a rapid progressive disease, compared to the proneural subtype. P-value, ANOVA-test (one-way analysis of variance). **f,** Types of collective glioma cell invasion in response to different microanatomy of brain subregions. Perivascular cohesive strands move through aligned confined space forming epithelial-like AJs whereas multicellular networks with dynamic and relatively short-lived neuronal-like filaments support intercellular connections during interstitial invasion of brain stroma. Black arrows, kinetics of cell-cell interactions. Blue arrows, direction of migration.

Supplementary Material

Refer to Web version on PubMed Central for supplementary material.

Acknowledgements

We acknowledge Esther Wagena, Manon Vullings, Krissie Lenting, Kiek Verrijp, Jeroen Mooren and Bianca Lemmers-Van de Weem for expert technical support in animal experiments, image analyses and immunohistochemistry. We further acknowledge Mirjam Zegers for critical reading of the manuscript.

Funding

This work was supported by The Netherlands Organization for Scientific Research (NWO-VICI 918.11.626), Pieken in the Delta Oost Nederland, the European Research Council (ERC-CoG DEEPINSIGHT, 617430), National Institutes of Health (U54 CA210184-01) and the Cancer Genomics Center, The Netherlands to P.F., and NWO-VENI (863.13.019) to C.E.J.D. and SFB834 to A.A.-P.

References

1. Wesseling P & Capper D WHO 2016 Classification of gliomas. Neuropathol. Appl. Neurobiol 44, 139–150 (2018). [PubMed: 28815663]
2. Network CGAR Comprehensive genomic characterization defines human glioblastoma genes and core pathways. Nature 455, 1061–1068 (2008). [PubMed: 18772890]
3. Frattini V et al. The integrated landscape of driver genomic alterations in glioblastoma. Nat. Genet 45, 1141–1149 (2013). [PubMed: 23917401]
4. Patel AP et al. Single-cell RNA-seq highlights intratumoral heterogeneity in primary glioblastoma. Science 344, 1396–1401 (2014). [PubMed: 24925914]
5. Brat DJ et al. Comprehensive, Integrative Genomic Analysis of Diffuse Lower-Grade Gliomas. N. Engl. J. Med 372, 2481–2498 (2015). [PubMed: 26061751]
6. Gilbert MR et al. Dose-dense temozolomide for newly diagnosed glioblastoma: a randomized phase III clinical trial. J. Clin. Oncol 31, 4085–4091 (2013). [PubMed: 24101040]
7. Stupp R et al. Effects of radiotherapy with concomitant and adjuvant temozolomide versus radiotherapy alone on survival in glioblastoma in a randomised phase III study: 5-year analysis of the EORTC-NCIC trial. Lancet. Oncol 10, 459–466 (2009). [PubMed: 19269895]
8. Montana V & Sontheimer H Bradykinin promotes the chemotactic invasion of primary brain tumors. J. Neurosci 31, 4858–4867 (2011). [PubMed: 21451024]
9. Cheng W-Y, Kandel JJ, Yamashiro DJ, Canoll P & Anastassiou D A multi-cancer mesenchymal transition gene expression signature is associated with prolonged time to recurrence in glioblastoma. PLoS One 7, e34705 (2012). [PubMed: 22493711]
10. Cuddapah VA, Robel S, Watkins S & Sontheimer H A neurocentric perspective on glioma invasion. Nat. Rev. Neurosci 15, 455–465 (2014). [PubMed: 24946761]
11. Gritsenko PG, Ilina O & Friedl P Interstitial guidance of cancer invasion. J. Pathol 226, 185–199 (2012). [PubMed: 22006671]
12. Osswald M et al. Brain tumour cells interconnect to a functional and resistant network. Nature 528, 93–98 (2015). [PubMed: 26536111]
13. Skalli O et al. Astrocytoma grade IV (glioblastoma multiforme) displays 3 subtypes with unique expression profiles of intermediate filament proteins. Hum. Pathol 44, 2081–2088 (2013). [PubMed: 23791210]
14. Claes A et al. Phenotypic and genotypic characterization of orthotopic human glioma models and its relevance for the study of anti-glioma therapy. Brain Pathol. 18, 423–433 (2008). [PubMed: 18371177]
15. Wang Q et al. Tumor Evolution of Glioma-Intrinsic Gene Expression Subtypes Associates with Immunological Changes in the Microenvironment. Cancer Cell 32, 42–56.e6 (2017). [PubMed: 28697342]
16. Chu Y, Hughes S & Chan-Ling T Differentiation and migration of astrocyte precursor cells and astrocytes in human fetal retina: relevance to optic nerve coloboma. FASEB J. Off. Publ. Fed. Am. Soc. Exp. Biol 15, 2013–2015 (2001).
17. Faber-Elman A, Solomon A, Abraham JA, Marikovsky M & Schwartz M Involvement of wound-associated factors in rat brain astrocyte migratory response to axonal injury: in vitro simulation. J. Clin. Invest 97, 162–171 (1996). [PubMed: 8550829]
18. Friedl P, Locker J, Sahai E & Segall JE Classifying collective cancer cell invasion. Nat. Cell Biol 14, 777–783 (2012). [PubMed: 22854810]
19. Peglion F, Llense F & Etienne-Manneville S Adherens junction treadmilling during collective migration. Nat. Cell Biol 16, 639–651 (2014). [PubMed: 24929360]
20. Sunyer R et al. Collective cell durotaxis emerges from long-range intercellular force transmission. Science 353, 1157–1161 (2016). [PubMed: 27609894]
21. Gritsenko P, Leenders W & Friedl P Recapitulating in vivo-like plasticity of glioma cell invasion along blood vessels and in astrocyte-rich stroma. Histochem. Cell Biol 148, 395–406 (2017). [PubMed: 28825130]

22. Serres E et al. Fibronectin expression in glioblastomas promotes cell cohesion, collective invasion of basement membrane in vitro and orthotopic tumor growth in mice. Oncogene 33, 3451–3462 (2014). [PubMed: 23912459]
23. Camand E, Peglion F, Osmani N, Sanson M & Etienne-Manneville S N-cadherin expression level modulates integrin-mediated polarity and strongly impacts on the speed and directionality of glial cell migration. J. Cell Sci 125, 844–857 (2012). [PubMed: 22275437]
24. Kolodkin AL & Tessier-Lavigne M Mechanisms and molecules of neuronal wiring: a primer. Cold Spring Harb. Perspect. Biol 3, (2011).
25. Hirano S & Takeichi M Cadherins in brain morphogenesis and wiring. Physiol. Rev 92, 597–634 (2012). [PubMed: 22535893]
26. Fujita Y & Yamashita T Axon growth inhibition by RhoA/ROCK in the central nervous system. Front. Neurosci 8, 338 (2014). [PubMed: 25374504]
27. Hensel N, Rademacher S & Claus P Chatting with the neighbors: crosstalk between Rho-kinase (ROCK) and other signaling pathways for treatment of neurological disorders. Front. Neurosci 9, 198 (2015). [PubMed: 26082680]
28. Chan C-H et al. Deciphering the transcriptional complex critical for RhoA gene expression and cancer metastasis. Nat. Cell Biol 12, 457–467 (2010). [PubMed: 20383141]
29. Muramatsu T et al. The hypusine cascade promotes cancer progression and metastasis through the regulation of RhoA in squamous cell carcinoma. Oncogene 35, 5304–5316 (2016). [PubMed: 27041563]
30. Watkins S & Sontheimer H Hydrodynamic cellular volume changes enable glioma cell invasion. J. Neurosci 31, 17250–17259 (2011). [PubMed: 22114291]
31. Harris TJC & Tepass U Adherens junctions: from molecules to morphogenesis. Nat. Rev. Mol. Cell Biol 11, 502–514 (2010). [PubMed: 20571587]
32. Gnanaguru G et al. Laminins containing the beta2 and gamma3 chains regulate astrocyte migration and angiogenesis in the retina. Development 140, 2050–2060 (2013). [PubMed: 23571221]
33. Weissman TA, Riquelme PA, Ivic L, Flint AC & Kriegstein AR Calcium waves propagate through radial glial cells and modulate proliferation in the developing neocortex. Neuron 43, 647–661 (2004). [PubMed: 15339647]
34. Fujii Y, Maekawa S & Morita M Astrocyte calcium waves propagate proximally by gap junction and distally by extracellular diffusion of ATP released from volume-regulated anion channels. Sci. Rep 7, 13115 (2017). [PubMed: 29030562]
35. Ozaki C et al. p120-Catenin is essential for N-cadherin-mediated formation of proper junctional structure, thereby establishing cell polarity in epithelial cells. Cell Struct. Funct 35, 81–94 (2010). [PubMed: 20859058]
36. Ishiyama N et al. Dynamic and static interactions between p120 catenin and E-cadherin regulate the stability of cell-cell adhesion. Cell 141, 117–128 (2010). [PubMed: 20371349]
37. Elia LP, Yamamoto M, Zang K & Reichardt LF p120 catenin regulates dendritic spine and synapse development through Rho-family GTPases and cadherins. Neuron 51, 43–56 (2006). [PubMed: 16815331]
38. Huveldt D et al. Targeting Src family kinases inhibits bevacizumab-induced glioma cell invasion. PLoS One 8, e56505 (2013). [PubMed: 23457577]
39. Schackmann RCJ, Tenhagen M, van de Ven RAH & Derksen PWB p120-catenin in cancer - mechanisms, models and opportunities for intervention. J. Cell Sci 126, 3515–3525 (2013). [PubMed: 23950111]
40. Anastasiadis PZ et al. Inhibition of RhoA by p120 catenin. Nat. Cell Biol 2, 637–644 (2000). [PubMed: 10980705]
41. van de Ven RAH et al. p120-catenin prevents multinucleation through control of MKLP1-dependent RhoA activity during cytokinesis. Nat. Commun 7, 13874 (2016). [PubMed: 28004812]
42. Friedl P & Alexander S Cancer invasion and the microenvironment: plasticity and reciprocity. Cell 147, 992–1009 (2011). [PubMed: 22118458]
43. Theveneau E & Mayor R Cadherins in collective cell migration of mesenchymal cells. Curr. Opin. Cell Biol 24, 677–684 (2012). [PubMed: 22944726]

44. Yang X, Hou D, Jiang W & Zhang C Intercellular protein-protein interactions at synapses. Protein Cell 5, 420–444 (2014). [PubMed: 24756565]
45. Verhaak RGW et al. Integrated genomic analysis identifies clinically relevant subtypes of glioblastoma characterized by abnormalities in PDGFRA, IDH1, EGFR, and NF1. Cancer Cell 17, 98–110 (2010). [PubMed: 20129251]
46. Gravendeel LAM et al. Intrinsic gene expression profiles of gliomas are a better predictor of survival than histology. Cancer Res. 69, 9065–9072 (2009). [PubMed: 19920198]
47. Venkataramani V et al. Glutamatergic synaptic input to glioma cells drives brain tumour progression. Nature 573, 532–538 (2019). [PubMed: 31534219]
48. Sloan SA & Barres BA Mechanisms of astrocyte development and their contributions to neurodevelopmental disorders. Curr. Opin. Neurobiol 27, 75–81 (2014). [PubMed: 24694749]
49. Dohn MR, Brown MV & Reynolds AB An essential role for p120-catenin in Src- and Rac1-mediated anchorage-independent cell growth. J. Cell Biol 184, 437–450 (2009). [PubMed: 19188496]
50. van de Ven RAH et al. Nuclear p120-catenin regulates the anoikis resistance of mouse lobular breast cancer cells through Kaiso-dependent Wnt11 expression. Dis. Model. Mech 8, 373–384 (2015). [PubMed: 25713299]
51. Schackmann RCJ et al. Cytosolic p120-catenin regulates growth of metastatic lobular carcinoma through Rock1-mediated anoikis resistance. J. Clin. Invest 121, 3176–3188 (2011). [PubMed: 21747168]
52. Bajrami I et al. E-Cadherin/ROS1 Inhibitor Synthetic Lethality in Breast Cancer. Cancer Discov. 8, 498–515 (2018). [PubMed: 29610289]
53. Padmanaban V et al. E-cadherin is required for metastasis in multiple models of breast cancer. Nature 573, 439–444 (2019). [PubMed: 31485072]
54. Cheung KJ, Gabrielson E, Werb Z & Ewald AJ Collective invasion in breast cancer requires a conserved basal epithelial program. Cell 155, 1639–1651 (2013). [PubMed: 24332913]
55. Te Boekhorst V & Friedl P Plasticity of Cancer Cell Invasion-Mechanisms and Implications for Therapy. Adv. Cancer Res 132, 209–264 (2016). [PubMed: 27613134]
56. Cooper JA Molecules and mechanisms that regulate multipolar migration in the intermediate zone. Front. Cell. Neurosci 8, 386 (2014). [PubMed: 25452716]
57. Barriga EH & Mayor R Embryonic cell-cell adhesion: a key player in collective neural crest migration. Curr. Top. Dev. Biol 112, 301–323 (2015). [PubMed: 25733144]
58. Kapitein LC & Hoogenraad CC Building the Neuronal Microtubule Cytoskeleton. Neuron 87, 492–506 (2015). [PubMed: 26247859]
59. Sakakibara A & Hatanaka Y Neuronal polarization in the developing cerebral cortex. Front. Neurosci 9, 116 (2015). [PubMed: 25904841]
60. Reffay M et al. Interplay of RhoA and mechanical forces in collective cell migration driven by leader cells. Nat. Cell Biol 16, 217–223 (2014). [PubMed: 24561621]
61. Zegers MM & Friedl P Rho GTPases in collective cell migration. Small GTPases 5, e28997 (2014). [PubMed: 25054920]
62. Chen C, Li PP, Madhavan R & Peng HB The function of p120 catenin in filopodial growth and synaptic vesicle clustering in neurons. Mol. Biol. Cell 23, 2680–2691 (2012). [PubMed: 22648172]
63. Hong JY, Oh I-H & McCrea PD Phosphorylation and isoform use in p120-catenin during development and tumorigenesis. Biochim. Biophys. Acta 1863, 102–114 (2016). [PubMed: 26477567]
64. McCrea PD & Gottardi CJ Beyond beta-catenin: prospects for a larger catenin network in the nucleus. Nat. Rev. Mol. Cell Biol 17, 55–64 (2016). [PubMed: 26580716]
65. Salinas PC Wnt signaling in the vertebrate central nervous system: from axon guidance to synaptic function. Cold Spring Harb. Perspect. Biol 4, (2012).

References

66. Gritsenko PG & Friedl P Adaptive adhesion systems mediate glioma cell invasion in complex environments. J. Cell Sci 131, 10.1242/jcs.216382 (2018).
67. Wurdinger T et al. A secreted luciferase for ex vivo monitoring of in vivo processes. Nat. Methods 5, 171–173 (2008). [PubMed: 18204457]
68. Mir SE et al. In silico analysis of kinase expression identifies WEE1 as a gatekeeper against mitotic catastrophe in glioblastoma. Cancer Cell 18, 244–257 (2010). [PubMed: 20832752]
69. Depner C et al. EphrinB2 repression through ZEB2 mediates tumour invasion and anti-angiogenic resistance. Nat. Commun 7, 12329 (2016). [PubMed: 27470974]
70. Sawamiphak S et al. Ephrin-B2 regulates VEGFR2 function in developmental and tumour angiogenesis. Nature 465, 487–491 (2010). [PubMed: 20445540]
71. Kitai R et al. Nestin expression in astrocytic tumors delineates tumor infiltration. Brain Tumor Pathol. 27, 17–21 (2010). [PubMed: 20425043]
72. Korff T & Augustin HG Integration of endothelial cells in multicellular spheroids prevents apoptosis and induces differentiation. J. Cell Biol 143, 1341–1352 (1998). [PubMed: 9832561]
73. Wu TD & Watanabe CK GMAP: a genomic mapping and alignment program for mRNA and EST sequences. Bioinformatics 21, 1859–1875 (2005). [PubMed: 15728110]
74. Anders S, Pyl PT & Huber W HTSeq--a Python framework to work with high-throughput sequencing data. Bioinformatics 31, 166–169 (2015). [PubMed: 25260700]
75. Anders S & Huber W Differential expression analysis for sequence count data. Genome Biol. 11, R106 (2010). [PubMed: 20979621]
76. Subramanian A et al. Gene set enrichment analysis: a knowledge-based approach for interpreting genome-wide expression profiles. Proc. Natl. Acad. Sci. U. S. A 102, 15545–15550 (2005). [PubMed: 16199517]
77. Mootha VK et al. PGC-1alpha-responsive genes involved in oxidative phosphorylation are coordinately downregulated in human diabetes. Nat. Genet 34, 267–273 (2003). [PubMed: 12808457]
78. Weissman TA, Riquelme PA, Ivic L, Flint AC & Kriegstein AR Calcium waves propagate through radial glial cells and modulate proliferation in the developing neocortex. Neuron 43, 647–661 (2004). [PubMed: 15339647]
79. Wu Y, Siadaty MS, Berens ME, Hampton GM & Theodorescu D Overlapping gene expression profiles of cell migration and tumor invasion in human bladder cancer identify metallothionein 1E and nicotinamide N-methyltransferase as novel regulators of cell migration. Oncogene 27, 6679–6689 (2008). [PubMed: 18724390]

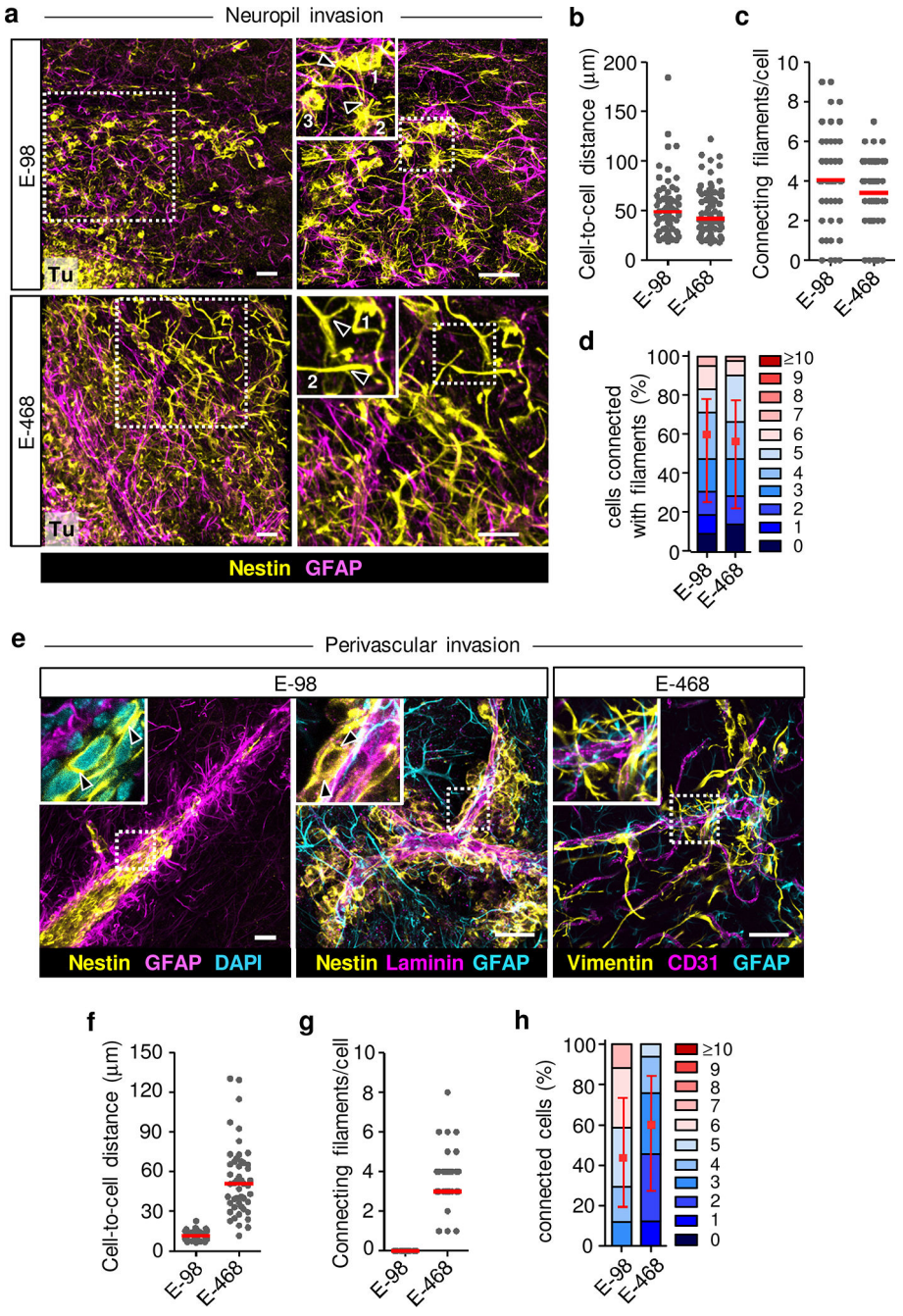

Figure 1. Multicellular glioma cell networks and perivascular invasion in mouse brain.

Morphological pattern and quantitative cell-cell junction analysis of interstitial networks (**a-d**) and perivascular invasion (**e-h)** in human glioblastoma xenografts. E-98 and E-468 cell lines were implanted into mouse brain and after 28 days peritumor regions were assessed by confocal microscopy (in 200 µm-thick brain slices). Identification of glioma cells by human nestin/vimentin staining. Brain stroma was detected by GFAP (astrocytes) and blood vessels by laminin or CD31 staining. Arrowheads indicate filamentous (a) or linear (e) contacts between glioma cells. Numbers in (a) indicate glioma cell bodies connected with filamentous cell protrusions. Tu, tumor. Example images in (a, e) represent tumors from 3

mice per PDX line. Data represent 63–79 (b), 42 (c, d), 36–48 (f) and 18–33 cells (g, h) from 2 representative mice from three independent implantation series. Scatter dot plots show the medians (red line) and values representing individual cells (b, c, f, g); in (d, h) values display relative fractions of connected glioma cells interacting with 0 up to ≥10 connected cells (boxes), median (red square), 25/75 percentiles (whiskers). Relative fractions of glioma cells connected with linear (E-98) or filamentous (E-468) junctions (h). Scale bars, 50 μm.

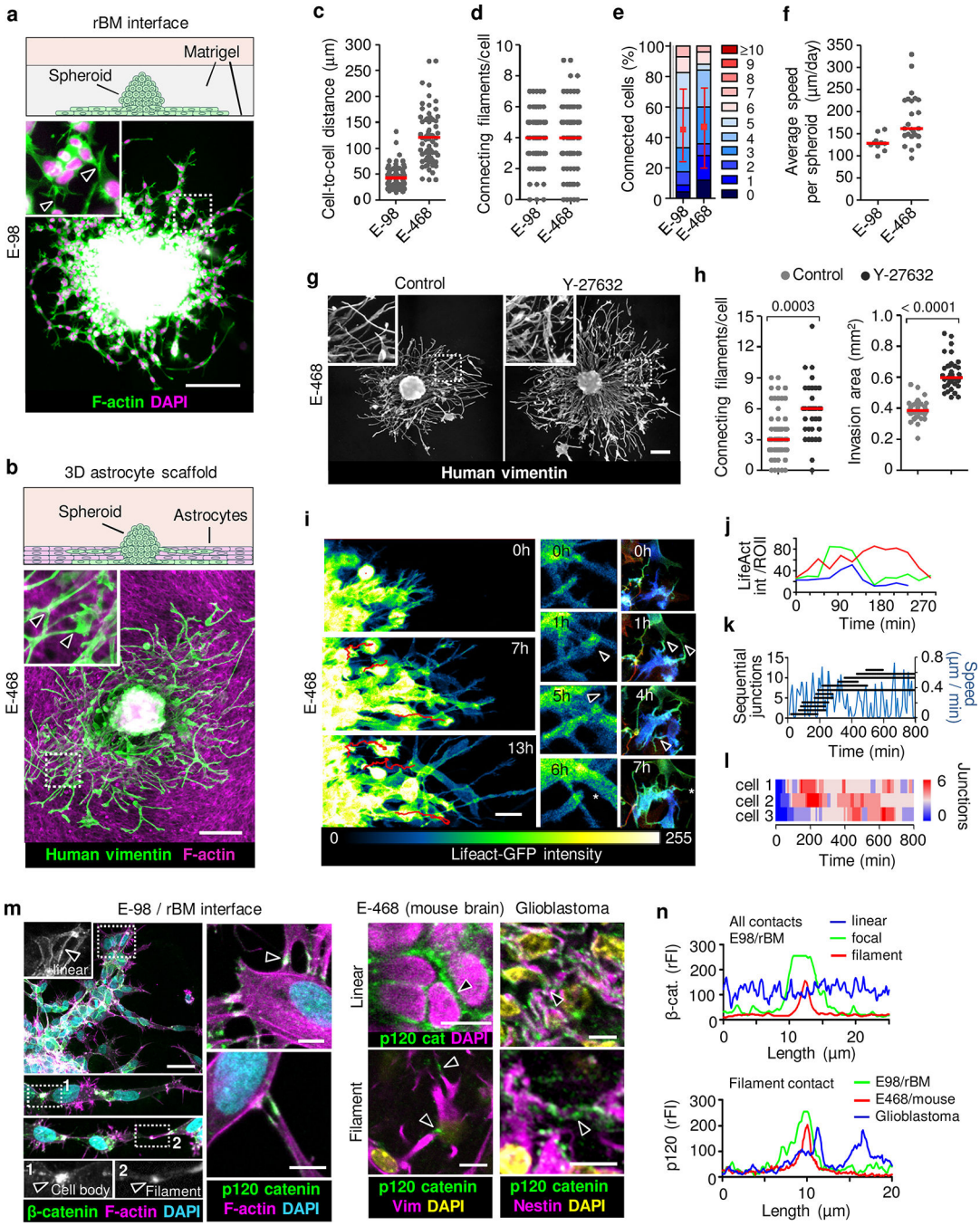

Figure 2. Collective glioma cell invasion in 3D assays and organization of cell-cell junctions during glioma network invasion.

Glioma spheroids in 3D environments including (**a**) the interface between two layers of reconstituted basement membranes (rBM) and (**b**) 3D astrocyte scaffolds after 48 h of invasion culture. Example images from 3 independent experiments. Arrowheads, filamentous cell-cell junctions. Quantification of next-neighbor proximity (**c**), number of cell-cell connecting filaments (**d**) or connected cells (**e**), and invasion speed (**f**) in astrocyte scaffold culture. Data represent 63–110 (c), 66–69 (d, e) cells and 10–24 spheroids (f) from

3 independent experiments. **g, h.** Glioma network invasion and ROCK inhibition. E-468 cell invasion in 3D astrocyte scaffolds in the absence (H_2O) or presence of ROCK inhibitor (Y-27632, 10 μM) after 48 h of culture. Data represent 34–52 (left) and 35–36 spheroids (right) per condition from 3 independent experiments. P values, two-tailed Mann-Whitney test. Scatter dot plots show individual cells (c, d; h, left) or spheroids (f; h, right) and medians (red line). Data in (e) display relative fractions of connected glioma cells interacting with 0 up to 10 connected cells (boxes), median (red square), 25/75 percentiles (whiskers). **i,** Time-sequence of actin dynamics. LifeAct/GFP-expressing E-468 spheroid culture on 3D astrocyte scaffolds. Formation (arrowheads) and resolution (asterisk) of cell-cell junctions. **j**, Intensity fluctuation of LifeAct/GFP in 3 representative filamentous cell-cell junctions over time (in Fig. 2i). **k,** Migration speed (blue line) while cell-cell junctions in single cell form and turn over. **l,** Steady-state number of intercellular connections in three moving cells (paths in Supplementary Video 5), represented as color bars. Data in (i-l) represent one out of 3 independent experiments. **m,** Heterogeneity of linear, focal and filamentous cell-cell interactions between glioma cells in vitro (m) and ex vivo (n). Samples were E-98 cells in rBM culture, n=3, E-468 xenografts in mouse brain, n=3 and clinical glioblastoma (top panels; 4 clinical $IDH1^{wt}$ glioblastoma samples). Arrowheads, β- and p120 catenin accumulation. **n**, β-catenin and p120 catenin fluorescence intensity (rFI) in linear-continuous or focal-filamentous cell-cell junctions. Scale bars, 200 μm (g), 50 μm (a-c; i; m, left panels) and 10 μm (m, right panels).

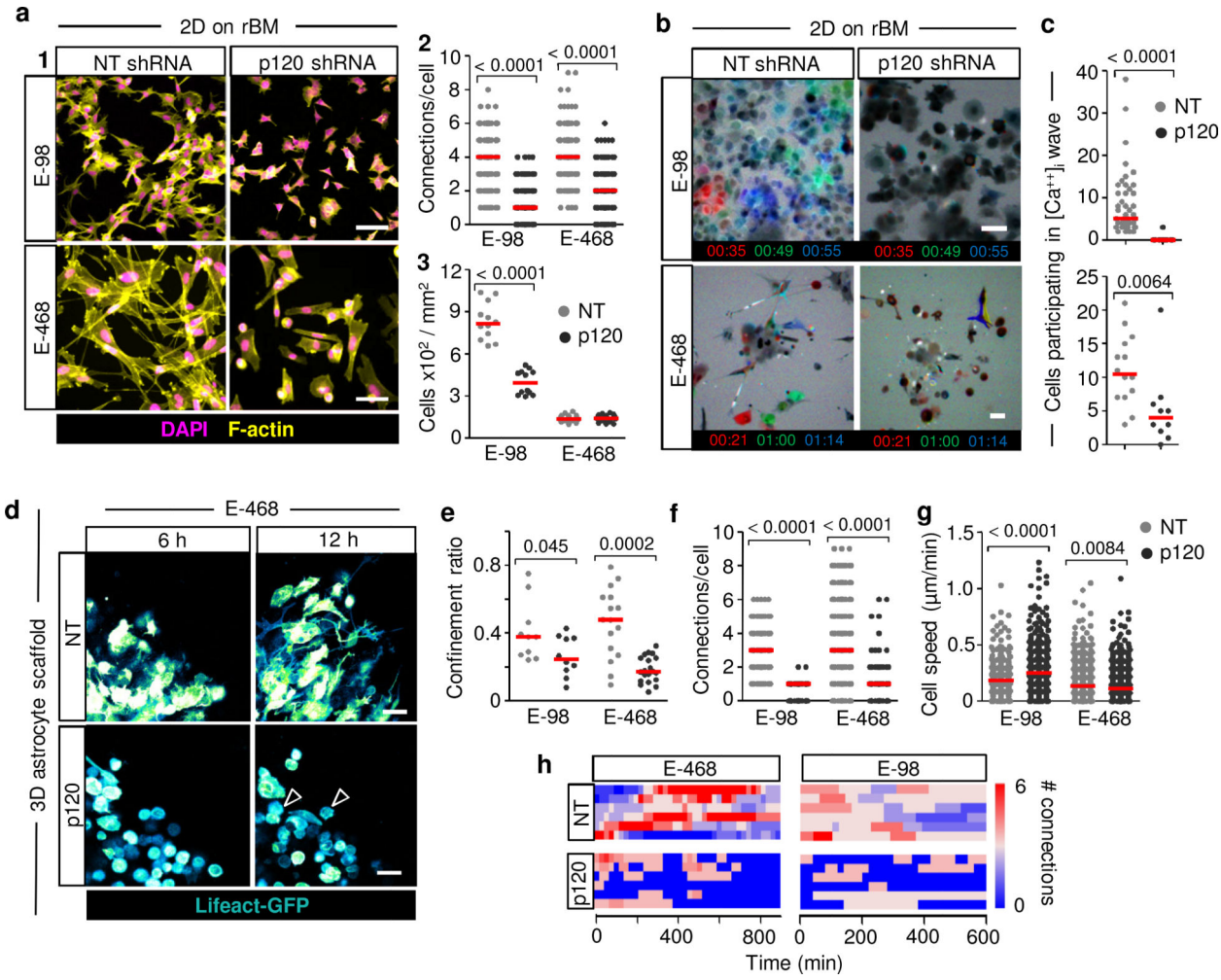

Figure 3. p120-dependent cell-cell cooperation and migration persistence of collective invasion of glioma cells.

a, Morphology (1), number of filamentous cell-contacts between neighboring cells (2) and cell growth (3) in response to stable expression of non-targeting (NT) and p120 shRNA in E-98 and E-468 cells on a culture plate coated with rBM. Data represent 196 to 226 cells (a2) and 12–18 cell areas (650×486 μm) from duplicate wells per condition from three independent shRNA lentiviral transductions. P values, two-tailed Mann-Whitney test. Efficiency, stability of downregulation and validation using independent shRNA probes are shown in Extended Data Fig. 5h–j. **b-h,** Impact of p120 downregulation on glioma cell network functions. **b, c,** Morphology and effect of p120 downregulation on calcium wave propagation between neighbor cells radially migrating from spheroids after 48h culture on rBM. Data in (b) show one out of 2 independent shRNA transductions. Data in (c) represent 10–19 spheroids per condition from 2 independent shRNA lentiviral transductions. P values, two-tailed Mann-Whitney test. **d,** Network kinetics (6- and 12- hours time-points) of E-468 cells expressing NT or p120 shRNA invading from spheroids into 3D astrocyte scaffolds. Arrowheads, non-polar cells deficient of protrusions and intercellular connections. Data represent 3 independent shRNA lentiviral transductions. **e-g**, Cell migration persistence, measured as confinement ratio (distance start-end point / total length of path) over a period

of 10–13 h (e); image-sequence based quantification of the median number of cell connections (f) and cell migration speed (g) on 3D astrocyte scaffolds after p120 downregulation, obtained by single cell tracking. Data represent 10–20 (e), 296–387 (f), 286–980 (g) cells from 6–8 movies each capturing 3 spheroids per condition from 3 independent shRNA transductions. P values, two-tailed Mann-Whitney test. **h,** Time-dependent cell-cell interactions in moving cells during 10–15h of migration. Scatter dot plots in (a2; e-g) show individual cells and median (red line). Scale bars, 100 μm (a), 50 μm (b, d).

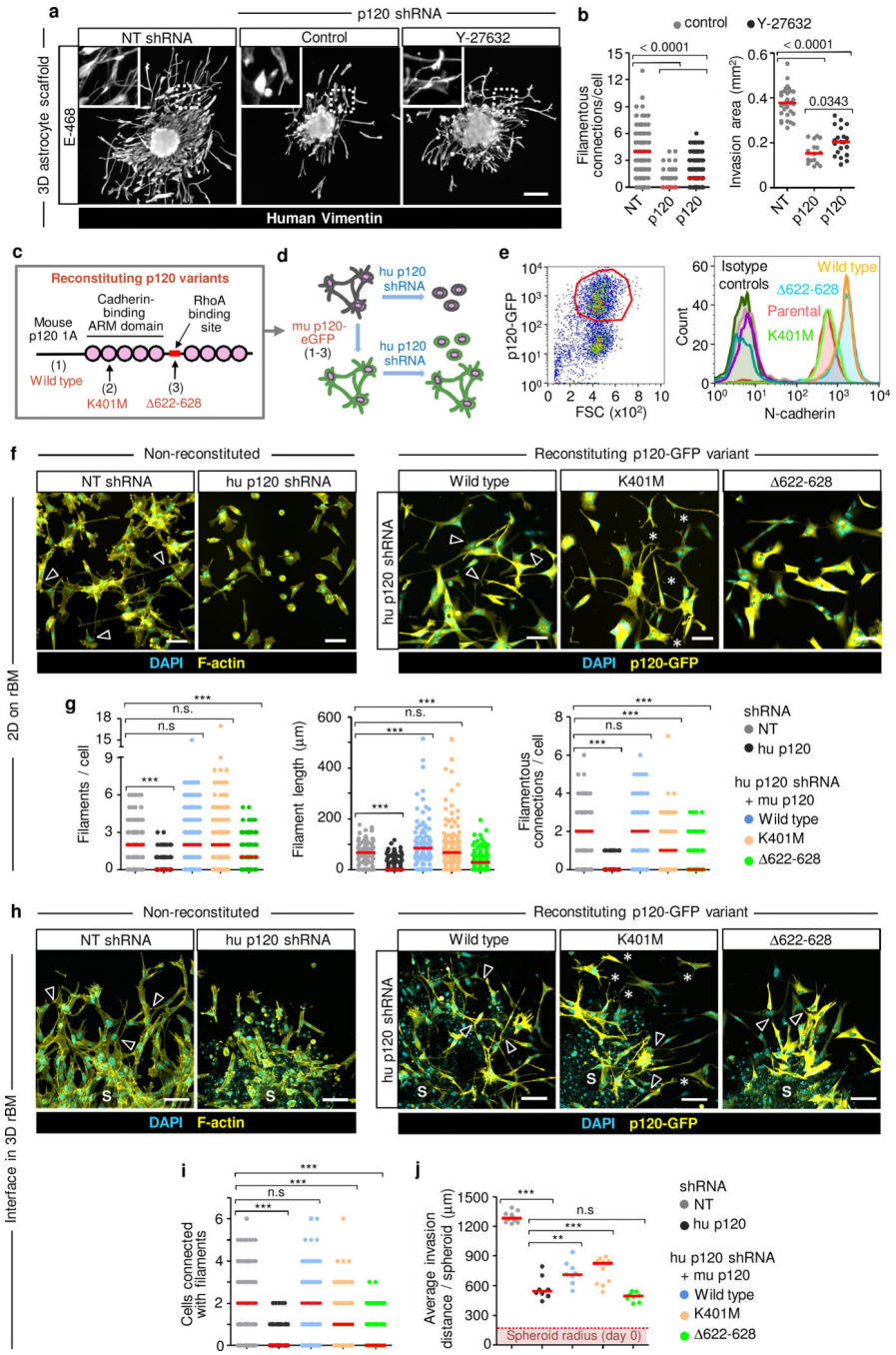

Figure 4. Multicellular network restitution after p120 downregulation and rescue with p120 domain mutants.

a, **b**, Filamentous connectivity and invasion efficiency of E-468 cells after 48h in 3D astrocyte culture. Conditions as described in Fig. 2g. Data represent 115–145 cells (left) and 16–32 spheroids (right) from 3 independent lentiviral transductions. P values, two-tailed Mann-Whitney test. **c**, Constructs encoding mouse p120 isoform 1A fused with eGFP. **d,** Expression of murine wild-type p120 (1), p120 K401M (2) or p120 Δ622–628 (3) in human glioma cells followed by transduction with p120 shRNA downregulating human p120. **e**.

Surface expression of N-cadherin in U-251 glioma cells transduced with constructs specified in (c). Gating strategy (left) and histograms of surface N-cadherin (right). Data show one of 2 independent experiments. **f**, Morphology of E-468 cells during 2D culture on rBM after transduction with p120 constructs indicated in (c). Arrowheads, filamentous cell-cell contacts. Asterisks, protrusions between neighbor cells without contact. Data show one of 3 independent experiments. **g**, Number and length of filamentous contacts between neighboring cells in p120 shRNA cells after re-expression of p120 catenin constructs indicated in (c), compared to non-targeting shRNA. Data represent 85–250 cells in duplicate wells per condition from 3 independent lentiviral transductions. P values, one-way ANOVA Dunnett's multiple comparison test; ***, P<0.0001. **h**, Morphology of E-468 cells expressing human p120 shRNA and transduction with human p120 constructs specified in (c) or non-targeting shRNA after 3 days of radial invasion from spheroids in 3D rBM interface culture. Arrowheads, filamentous cell-cell contacts. Asterisks, regions with protrusions between neighbor cells without contact. S, spheroids. **i,** Number of cells connected with filamentous protrusions. **j,** Average distance of the invasion edge from the spheroid center. Conditions in (i, j) as described in (h). Data represent 144–175 cells from 6–8 spheroids (i) or 8–12 spheroids (j) per condition from 2 independent transductions. P values, one-way ANOVA Dunnett's multiple comparison test; ***, P<0.0001, **, P <0.01. Scatter plots show individual cells (b, left graph; g, j) or the means from individual spheroids (b, right graph; j) and medians (red line). Scale bars, 200 μm (a), 100 μm (f, h).

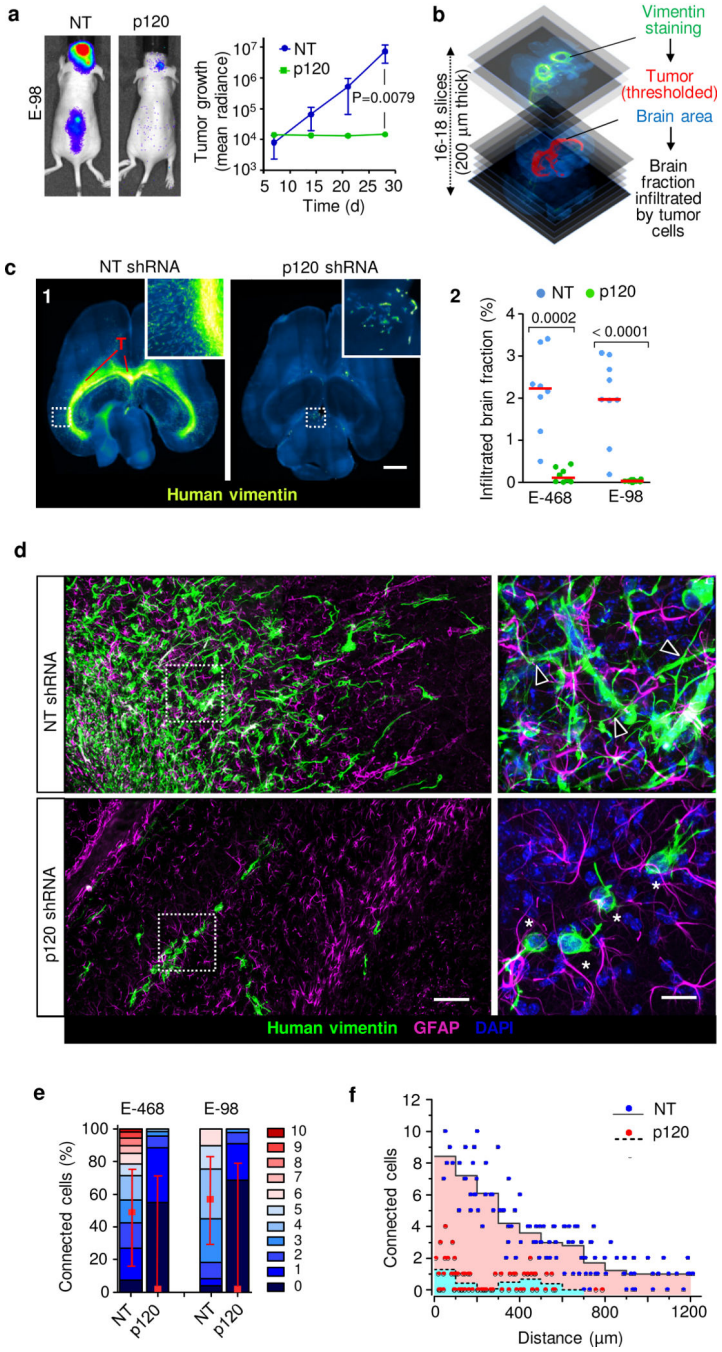

Figure 5. p120 is indispensable for glioma growth, network formation and diffuse brain infiltration.

a, Bioluminescence distribution and intensity after implantation into the mouse brain. Data represent the means and ±SEM from 5 mice/group. P value (day 28), two-tailed Mann-Whitney test. **b**, Ex-vivo technique to quantify the mouse brain volume infiltrated with glioma cells. **c1,** Impaired tumor growth and diffuse brain infiltration of E-468 cells after p120 downregulation. Overviews and detail (insets) from 200 µm thick brain slices. **c2,** Extent of brain volume consumption by E-468 and E-68 glioma cell lines, expressed as

cumulative percent of brain section area containing vimentin-positive glioma cells 4 weeks post-implantation. Scatter dot plots show the medians (red line) and data from individual brains from 19 (E-98) and 16 (E-468) mice from two independent implantation series. P values, two-tailed Mann-Whitney test. **d,** Diffuse brain infiltration of E-468 cells as multicellular networks and perturbation after p120 downregulation 30 days post-implantation (3D confocal microscopy from 200 μm thick brain slices). Mouse astrocytes are visualized with GFAP staining. Arrowheads, vimentin-positive filamentous protrusions in multicellular glioma networks. Asterisks, single glioma cells. Similar results were observed in 8 mice per condition from two independent implantation series. **e,** Perturbation of cell-cell interactions in two glioma models in 4 weeks post-implantation. Data represent 49–108 cells from two mice per condition from two independent implantation series. Relative fractions of connected glioma cells interacting with 0 up to 10 connected cells (boxes), median (red square), 25/75 percentiles (whiskers). **f,** Frequency of cell-cell junctions from the region of maximum cell density (“0”) to the front of the diffuse infiltration zone covering 1200 μm in E-468 cells expressing NT or p120 shRNA. Scale bars, 2 mm (c1), 100 μm (d, overview), 25 μm (d, detail).

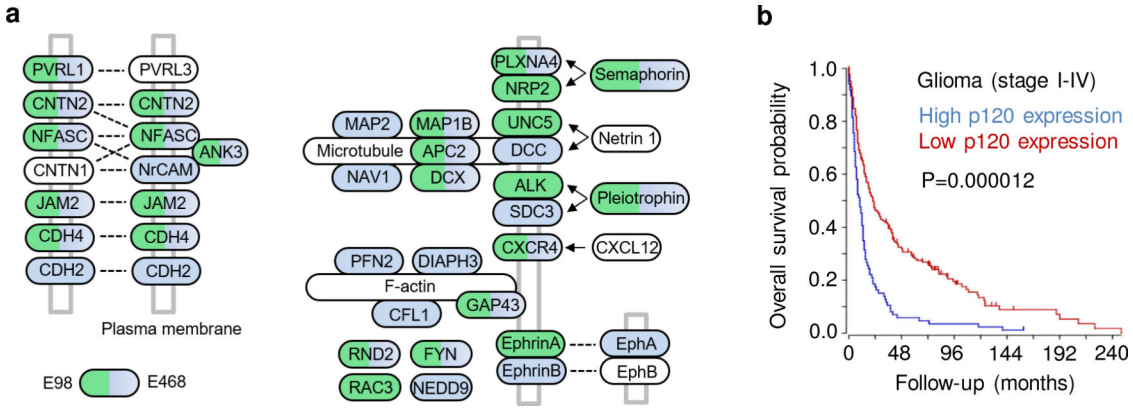

Figure 6. Neuronal related pathways regulated by p120 catenin in glioma cells and clinical relevance in glioma patients.

a, Deregulated cell adhesion and axon guidance after downregulation of p120 catenin in glioma cells, based on Gene Ontology term analysis and the KEGG network maps “Cell-cell adhesion” and “Axonogenesis” biological functions. Pathway-related genes significantly down-regulated in E-98 or E-468 cell lines upon p120 shRNA targeting are annotated in respective green or blue fillings. The underlying RNA expression analysis and clustering are shown in Extended Data Fig. 8a, b and Supplementary Table 2. **b**, Overall survival of glioma patients (grade I – IV) with high or low p120 mRNA expression (French dataset[46], n=284 patients). P values, two-tailed Mann-Whitney test, Bonferroni corrected.